To the Graduate Council:

I am submitting herewith a thesis written by John Dirk Richards entitled "ON THE DETECTION OF TWO ELECTRONS IN LOW-LYING CONTINUUM STATES OF A SINGLE PROJECTILE ION RESULTING FROM THE COLLISION OF A 10.7 MeV AG^{4+} ION WITH AN AR GAS TARGET." I have examined the final copy of this thesis for form and content and recommend that it be accepted in partial fulfillment of the requirements for the degree of Masters of Science, with a major in Physics.

Marianne Breinig

Marianne Breinig, Major Professor

We have read this thesis
and recommend its acceptance:

Leo L. Riedinger

Accepted for the council:

Associate Vice Chancellor
and Dean of The Graduate School

STATEMENT OF PERMISSION TO USE

In presenting this thesis in partial fulfillment of the requirements for a Master's degree at The University of Tennessee, Knoxville, I agree that the Library shall make it available to borrowers under the rules of the Library. Brief quotations from this thesis are allowable without the special permission, provided that accurate acknowledgement of the source is made.

Permission for extensive quotation from or reproduction of this thesis may be granted by my major professor, or in her absence, by the Head of Interlibrary Services when, in the opinion of either, the proposed use of the material is for scholarly purposes. Any copying or use of the material in this thesis for financial gain shall not be allowed without my written permission.

Signature______________________________

Date______________________________

ON THE DETECTION OF TWO ELECTRONS IN LOW-LYING CONTINUUM STATES OF A SINGLE PROJECTILE ION RESULTING FROM THE COLLISION OF A 10.7 MeV AG^{4+} ION WITH AN AR GAS TARGET

A Thesis

Presented for the

Master of Science

Degree

The University of Tennessee, Knoxville

John Dirk Richards

May 1992

DEDICATED TO

MY PARENTS

AND

MY SISTERS

ACKNOWLEDGEMENTS

In conducting the experimental research reported in this thesis, I am indebted to my major professor Dr. Marianne Breinig, to fellow students C. C. Gaither III, Brian Hasson and John Berryman, and to other members of the University of Tennessee Atomic Physics group and staff of the Oak Ridge National Laboratory EN tandem accelerator facility who assisted with the experiments. In addition, I wish to thank Dr. Breinig for her unending effort in editing my written work and her continued support, during the past three years, which allowed this phase of the project to be completed.

I wish to thank Professors David Pegg, and Lee Riedinger, members of my committee, for taking time away from their busy schedules to review my thesis.

Finally I wish to thank Rowdy and Lois Busch, and Phil Benson for their support and assistance in preparing the talk I presented on this experiment in the Fall of 1991.

ABSTRACT

An important problem in atomic dynamics which may require treatment beyond the independent particle model is the structure of high energy doubly-excited states, in which two electrons are simultaneously excited away from the rest of the electrons in the ionic core, making their mutual interaction as important as their individual interaction with the remaining core. This thesis reports on an atomic collision experiment which investigates the feasibility of using a large 30° parallel plate electrostatic analyzer to detect two electrons in low lying continuum states of a projectile ion. The two electrons are excited just above the double ionization threshold of a Ag^{q+} projectile ion in a collision of a 0.1 MeV/u Ag^{4+} ion with an Ar atom. The analyzer is used to deflect the free electrons which move with approximately the projectile velocity into a detector. The electron detector consists of electrically isolated anode segments located behind a microchannel plate electron multiplier.

We have measured the cross sections for producing states with one electron moving with a kinetic energy less than 0.13 eV in the projectile frame and the other moving with somewhat higher kinetic energy. To the best of our knowledge the present work describes the first sucessful measurement of this kind. The results of our measurements

may signal electron-electron correlation effects. We have shown that electrons moving with kinetic energies between 0.18 eV and 0.35 eV in the projectile frame are more likely to move perpendicular than antiparallel to the beam direction if another very low energy continuum electron is present. Otherwise the angular distribution of the electrons, in this energy range, is more isotropic.

TABLE OF CONTENTS

LIST OF TABLES

LIST OF FIGURES

FIGURE

CHAPTER 1

INTRODUCTION

For ion-atom collisions, single electron transitions and many multiple electron events have been successfully described by the independent particle model (IPM). This model describes each electron in the atomic system as moving in an effective potential comprised of the attractive Coulomb potential of the nuclei and the average repulsive potential of the other electrons present. Consequently, the IPM neglects the possibility of electron-electron correlation, i.e. the non-central component of the electron-electron Coulomb interaction between any two electrons. The effects of electron-electron interactions included in the calculations of probability amplitudes for ion-atom collisions produce two types of electron correlation as outlined by McGuire: static correlation which is contained in the asymptotic wave functions, i.e. in the wave functions of the initial and final state, and scattering correlation which occurs during the collision and is contained in the evolution operator for the system[1].

An important problem in atomic dynamics, which may require treatment beyond the independent particle model, is the structure of high energy doubly-excited states, in which two electrons are simultaneously excited away from the rest of the electrons in the ionic core, making their mutual interaction as important as their individual interaction with the remaining core.[2,3] This thesis reports on the results of an atomic collision experiment which investigates the feasibility of using a particular apparatus to detect two electrons in low-lying continuum states of a projectile ion. The two electrons are excited just above the double ionization threshold of a Ag^{q+} projectile ion in a collision of a 0.1 MeV/u Ag^{4+} ion with an Ar atom. We will briefly outline current theories concerning the behavior of two electrons in low-lying continuum states of the same ion.

In 1948, two-body threshold laws were investigated by Wigner.[4] A key result of his paper is that if a pair of particles is formed with near-zero asymptotic relative kinetic energy then the energy dependence of the cross section for the formation of this two-body threshold state is a function of the long-range potential between the particles only and is independent of the reaction mechanism responsible for its formation. If the dominant long range potential is an attractive Coulomb potential, then the singly differential cross section, $d\sigma/dE$, is a constant. For the production of a single electron in a low-lying continuum state of a projectile ion we therefore have $d\sigma/dE$ = constant or $d\sigma/d\vec{v} \propto 1/v$ as long as the energy E above the ionization limit is close to threshold. The electron density in velocity space diverges as the velocity of the electron in the projectile frame goes to zero. The laboratory frame energy distribution of electrons, emitted into a cone of half angle θ_0 about the beam direction, subsequently, exhibits a cusp-shaped peak centered at the energy of an electron moving with the projectile velocity. Electrons transferred into low-lying continuum states of the projectile in ion-atom collisions are therefore often referred to as cusp electrons.[5]

Gregory Wannier in 1953 derived a threshold law for the formation of final states consisting of three charged bodies, for example, two electrons and a positively charged ionic core.[6] He considered the problem of single ionization of atoms or ions by electrons. Near threshold he was able to reduce the general quantum problem of three bodies to a classical analysis with particular emphasis upon asymptotic properties of orbits of small positive energy. Wannier showed that all orbits initially symmetric in the two electrons lead to the escape of both particles.[6] Such states are now commonly referred to as ridge states. Wannier's treatment gives the energy dependence of the cross section for the formation of such three-body final states near threshold as

$$\sigma(E) \propto E^{\frac{1}{2}\mu-\frac{1}{4}} \tag{1.1}$$

where

$$\mu=\frac{1}{2}\left[\frac{100Z-9}{4Z-1}\right]^{\frac{1}{2}}, \tag{1.2}$$

E is the total energy of the three-body system and Z is the effective charge of the core.[6] The Wannier theory makes specific predictions about energy and angular correlations between outgoing electrons. While most other models for the double escape of two electrons from a positive core distinguish between the two electrons and predict that an exactly equal partition of E into E_1 and E_2 is less likely than any unequal partition, the Wannier theory predicts that all possible partitions become equally likely near threshold.[7] Angular correlations are predicted to be an extreme near threshold. The electrons are moving slowly and their mutual repulsion makes them likely to end up on opposite sides of the positively charged core.[8]

Ridge states are not the only possible states for two electrons near threshold. In the case of valley states or planetary states the initial orbits are not symmetric in the two electrons, i.e. one electron is initially closer to the core than the other. An interesting question is which types of states, valley or ridge states, dominate in the continuum just above threshold.[9] Experiments exploring the behavior of two electrons in low-lying continuum states near threshold-ionization have been performed successfully by singly ionizing target atoms in collisions with electrons and by doubly ionizing target atoms with a single photon. Results of these experiments thus far verify Wannier's threshold law.[10-12] To our knowledge no previous experiment has been performed to measure the behavior of two free electrons in low-lying continuum states of the projectile following a collision with a target atom.

In recent years many investigators have studied various two-electron transitions in ion-atom collisions. While the IPM describes most single-electron transitions well, experimental evidence suggests that electron-electron correlation must be included in the description of two-electron transitions. For example, two-electron transitions in helium have been found to be strongly influenced by electron correlation effects, and double excitation/ionization of helium in fast ion-atom collisions has recently received much attention, both experimentally and theoretically.[13-18] Other investigators have studied the formation of non-equivalent electron configurations in the double capture of target electrons to investigate electron-electron interactions.[19-22] In addition, the manifestation of electron-electron correlation in the transfer ionization process has been extensively investigated.[23-27]

This experiment is a feasibility study. We are attempting to detect two electrons independently, in low-lying continuum states of a 0.1 MeV/u Ag^{q+} projectile ion following a collision of a Ag^{4+} ion with an argon gas target under single collision conditions and to explore in a limited way their energy and angular correlations. A related experiment has been performed previously. It involved the detection of a cusp electron in coincidence with an electron in a high Rydberg state of the same projectile ion. As in the present experiment, 0.1 MeV/u Ag^{4+} projectile ions were incident on Ar, He and H_2 gas targets. The energy distribution of the cusp electrons was measured with and without the Rydberg coincidence requirement. The width was seen to narrow with the coincidence requirement imposed for two of the gas targets, H_2 and Ar, possibly signaling a correlation effect.[28]

CHAPTER 2

EXPERIMENTAL APPARATUS

A. OVERVIEW OF THE EXPERIMENT

In this experiment, collimated 0.1 MeV/u Ag^{4+} ions collide with a neutral Ar gas target. The center of the gas cell is located at the entrance focus of a large 30° parallel plate electrostatic analyzer. This analyzer is used to deflect free electrons in low-energy continuum states of the projectile, i.e. electrons which move with approximately the projectile velocity, into a detector. These electrons are either produced by projectile ionization or by target electron capture to the continuum and are often referred to as cusp electrons.[5] Projectile ions pass nearly undeflected through the 30° analyzer and are separated downstream according to exit charge state in a charge state analyzer and detected in a particle detector. The electron detector consists of electrically-isolated anode segments located behind a microchannel plate electron multiplier. This system is capable of simultaneously detecting two electrons in low-energy continuum states of the same projectile ion, when these electrons strike the microchannel plate above two different anode segments. The two segments then produce pulses at the same time and a coincidence is recorded. In order to determine the production mechanism and to eliminate background coincidences due to two electrons not moving with the appropriate speed, we record only electron-electron coincidences that precede the detection of a projectile ion by the difference in flight times between the electrons and the ion. By appropriately delaying the electron signals we require that each electron signal overlap the signal of the corresponding ion of exit charge state q thus enacting a triple coincidence measurement. In the following sections the experimental apparatus will be described in detail.

B. GENERAL LAYOUT OF THE EXPERIMENT

The experiment is carried out using the ORNL tandem Van de Graaff accelerator. The experimental layout is illustrated in figure 2.1. A beam of positively charged Ag ions is generated using a terminal voltage such that Ag^{4+} ions have an energy of 0.1 MeV/u. The analyzing magnet passes only the Ag^{4+} ions and the switching magnet directs them down the beamline towards the experimental chamber. Before the beam reaches the chamber and the experimental apparatus, it is collimated with two 0.5 mm apertures located 165 cm and 35 cm in front of the gas target, respectively. This ensures a beam divergence of less than 0.2 mrad and a beam spot size less than 0.8 mm diameter on

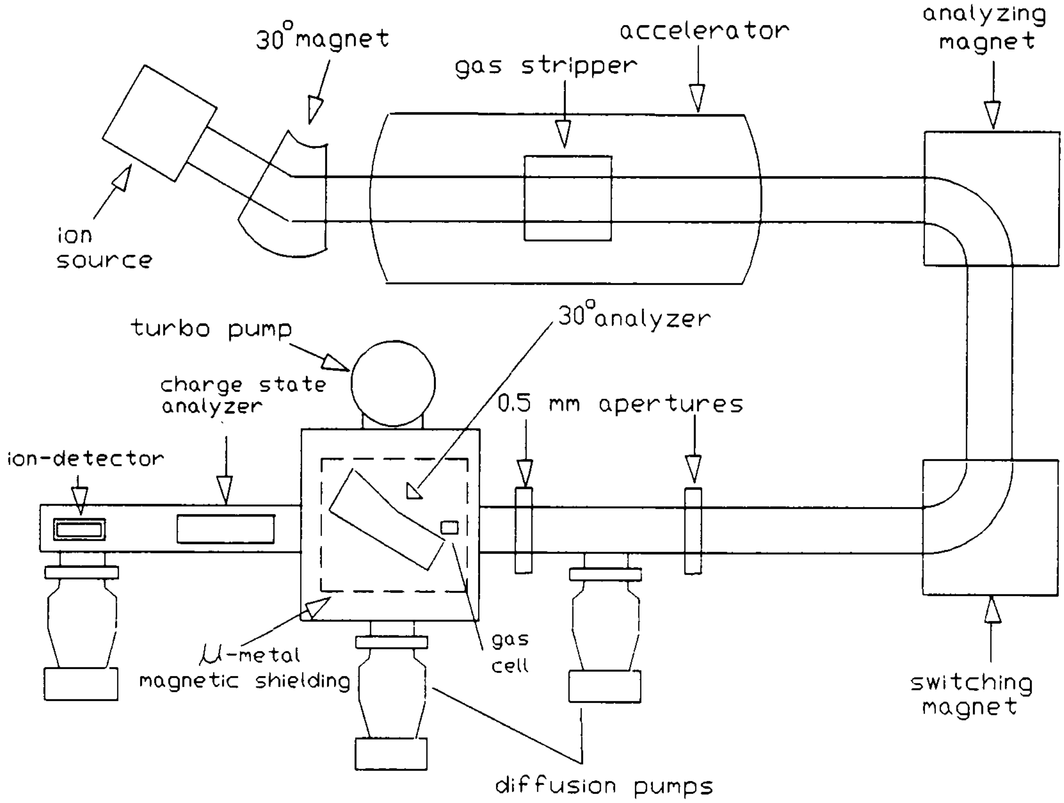

Figure 2.1 Schematic diagram of EN tandem Van de Graaff accelerator and experimental beamline

target. The pressure in the beam line is maintained by a cryo pump and a diffusion pump and the background pressure is less than 5×10^{-7} torr. In the experimental chamber the Ag^{4+} ions collide with argon atoms in the gas cell. The gas cell has an estimated effective length of 1.53 cm and is centered at the entrance focus of the 30° electrostatic analyzer. The pressure in the chamber is maintained by a turbo pump and a diffusion pump and the background pressure is less than 3×10^{-6} torr. The 30° analyzer deflects free electrons produced in the collision towards a detector. Because the free electrons are strongly affected by stray magnetic fields the entire experimental apparatus inside the chamber is enclosed in a μ-metal housing. The beam passes nearly undeflected through the 30° analyzer into the charge state analyzer where Ag ions of a particular exit charge state are directed into the particle detector, a discrete-dynode electron multiplier. The pressure in the region containing the charge state analyzer and the ion detector is maintained by a large diffusion pump, and is less than 2×10^{-7} torr.

C. 30° ELECTROSTATIC ANALYZER: GENERAL PROPERTIES

Electrons emerging nearly undeflected from the interaction region with a velocity close to the beam velocity enter the large 30° parallel plate electrostatic analyzer. The center of the gas cell coincides with the entrance focus of the analyzer. The gas cell and the base plate of the analyzer are grounded. Typically, a 30° parallel plate electron energy analyzer consists of a grounded plate and a high-voltage plate held at a negative potential, V. The electric field between the plates deflects the electrons. Figure 2.2 schematically shows a cut through a 30° parallel-plate electrostatic energy analyzer.[29] The cut is made perpendicular to the parallel plates and contains the entrance focus. The projection of an electron trajectory making an angle $\theta = 30°$ with the ground-plate is also shown. A 30° analyzer is second-order focussing in the plane of the cut. Electrons with the same velocity component in the plane of the cut leave the entrance focus, with trajectories whose projections onto the plane of the cut make an angle $\theta \pm \Delta\theta$ with the ground-plate are focussed onto a line in the focal plane. This line is perpendicular to the plane of deflection. Electrons with different velocity components in the plane of the cut are focused onto different parallel lines. Their position along these focal lines is determined by their emission angle perpendicular to the plane of deflection. For a 30° analyzer the focal plane makes an angle $\alpha = 10.9°$ with the ground-plate. If the acceptance angle in the plane of deflection is limited to a narrow range of angles about 30° but a wide range of angles is accepted perpendicular to the

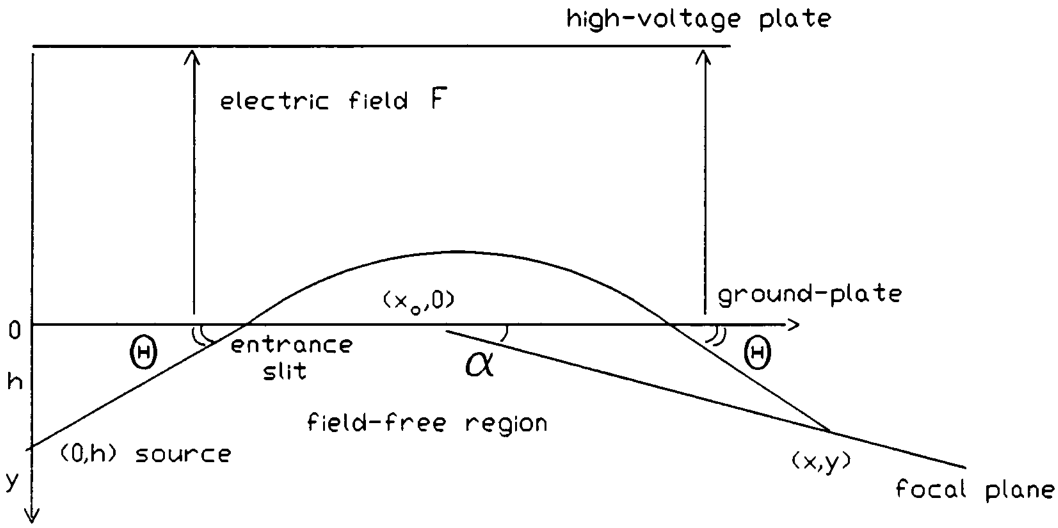

Figure 2.2 A cut through a 30° parallel plate electrostatic analyzer. The source is mounted at (0,h) in the field-free space. The mean ray makes an angle θ to the x axis.

plane of deflection then, in the focal plane, the energy andthe angular distribution of electrons emitted in a plane perpendicular to the plane of deflection will be imaged. Distances along the focal plane from the intersection of the focal plane with the ground-plate (from (x_o, 0) to (x, y) in figure 2.2) correspond to the velocity component of the electrons in the plane of the cut, while distances away from the cut are proportional to the velocity component perpendicular to the plane of the cut, i.e. to the laboratory frame emission angle. The x-component of the total trajectory of an electron from the source point to the focal plane is given by,

$$x=(h+y)\cot\theta+\left(\frac{2T}{F}\right)\sin(2\theta) \tag{2.1}$$

Here Θ ,x(cm), h(cm) and y(cm) are defined in figure 2.2 and T(eV) is defined as

$$T=\frac{1}{2}m_e v_c^2 \tag{2.2}$$

where v_c is the electron velocity component in the plane of the cut. Note that T is not the kinetic energy of the electron unless its velocity component perpendicular to the plane of the cut is zero. F(V/cm) denotes the electric field between the plates. Differentiating Eq. 2.1 with respect to θ and setting $dx/d\theta = 0$ one obtains

$$h+y=4\frac{T}{F}\sin^2\theta\cos2\theta \qquad (2.3)$$

Using eq. 2.3 to eliminate T/F from eq. 2.1 one finds the equation for the line of energy foci in the plane of the cut,

$$x=(h+y)\cot\theta\left(1+\frac{1}{\cos2\theta}\right) \qquad (2.4)$$

Table 2.1 gives the dimensions and other relevant parameters of the 30° analyzer used in our experiments.

D. ANALYZER MODIFICATIONS

The large 30° analyzer used in this experiment has been previously used and described by Freyou et al.[30] The analyzer's cross sectional view is shown in figure 2.3 and its dimensions are given in table 2.1. The exterior structure of the analyzer is not changed. The goal of the modifications is to reduce the number of background electrons reaching the detector. The microchannel plate mount has been remade with an edge beveled at the same angle

Table 2.1

Relevant parameters for the 30° parallel plate electron spectrometer.

Parameter	Value
Focal plane pivot point	x_o = 15.1 cm
Y distance from source to field region	h = 2.9 cm
Distance between earth plate and mid plane grid	d = 2.77 cm
Distance between fringe field plates	s = 6.0 mm
Focal plane pivot angle	α = 10.9°
Central angle of acceptance	Θ = 30° -3.01°, +3.26°
Transverse angle of acceptance	β = ± 10°
Energy acceptance range	E_{max}/E_{min} = 1.42

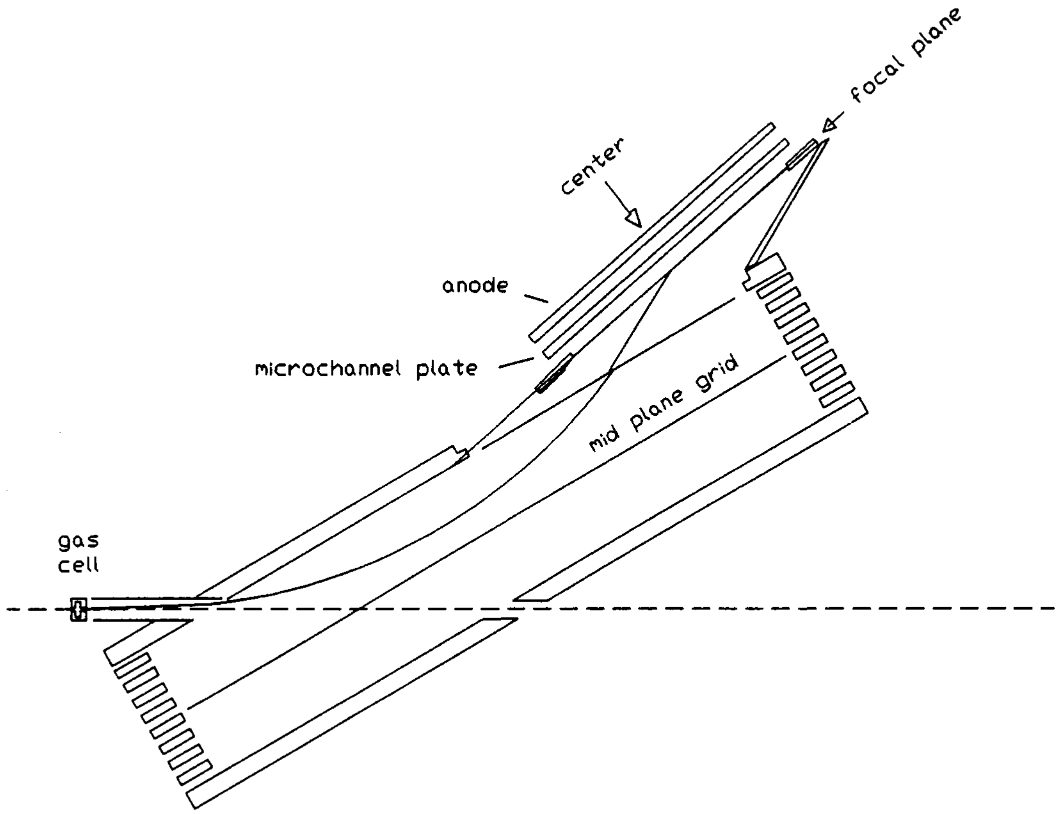

Figure 2.3 A cross sectional view of the 30° analyzer used in our experiment

at which electrons pass on their way to the detector region(see figure 2.4). This removes a source of secondary electrons which can reach the detector and contribute to the background in the low energy part of the energy spectrum measured with the microchannel plate detector. The midplane grid shown in figure 2.3 acts as an effective back plate and is held at a negative potential. The top and the bottom plate of the analyzer are grounded. The grid is positioned as close to the bottom plate as possible so that the trajectories of the highest energy electrons that can reach the detector just pass below the grid. Trajectories of electrons with the higher energy intersect the grid at a point from which ejected electrons are accelerated towards the ground plate and not towards the detector.

The three transmission grids used in the analyzer, the midplane grid, the ground-plate grid and the focal plane grid have been improved upon. Instead of using industrially woven screens we now construct a grid with wires running only in one direction as illustrated in figure 2.5. The wires are spaced 3 mm apart to maximize transmission while still preserving a uniform electric field. The grids made in this way increase transmission and almost completely eliminate background generated by electrons hitting grid material.

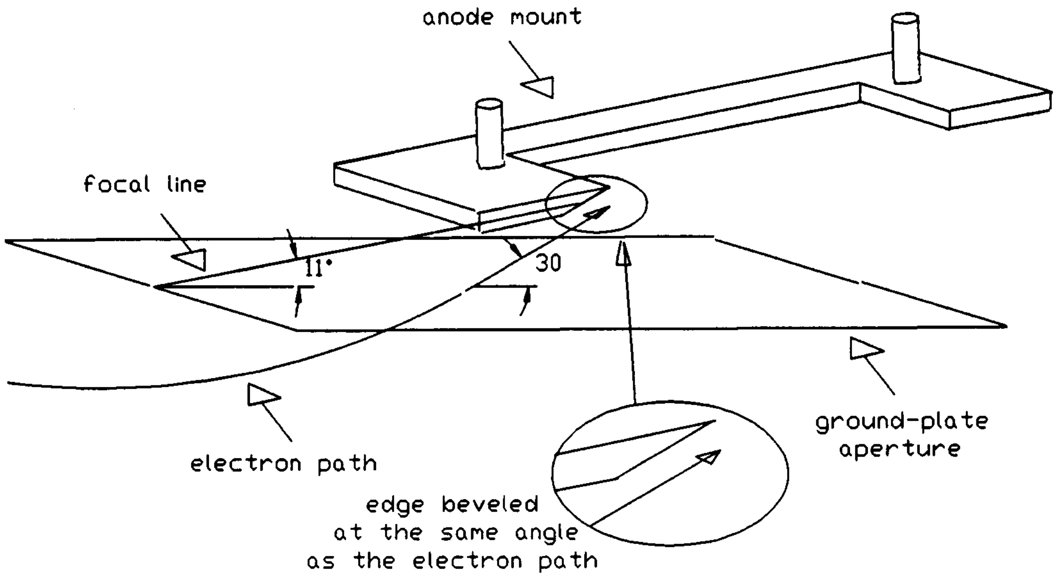

Figure 2.4 A 3-D view of the anode mount located in the focal plane of the analyzer with the cut showing the beveled edge.

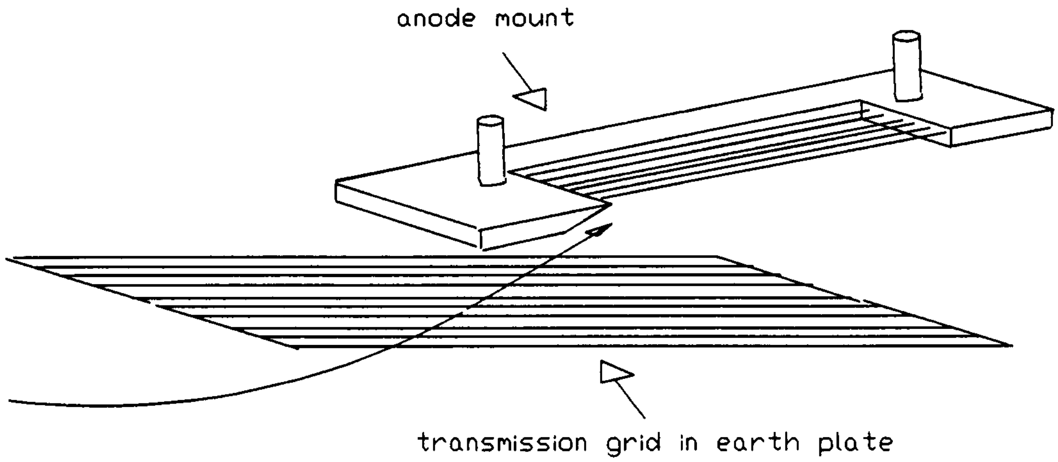

Figure 2.5 A 3-D view of the anode mount depicting the orientation of the 0.001 inch diameter tungsten wire grid on the anode mount and the ground-plane.

E. SPECIFIC ANALYZER PROPERTIES

For a 30^{o} parallel plate spectrometer, chose the x-axis as shown in figure 2.2, and chose a potential difference V yielding an electric field F between the parallel plates. Then the x-component of an electron's path from the gas cell to where it crosses the focal plane depends to second order only on the component of the electron's laboratory frame velocity in the plane of the cut. Setting $\theta = 30^{o}$ in eq.2.3 yields

$$h+y=.5\left(\frac{T}{F}\right). \tag{2.5}$$

Inserting equation 2.5 into equation 2.1 yields for the x-component of the electron's path

$$x=2.5981\left(\frac{T}{F}\right) \tag{2.6}$$

where T is defined in eq. 2.2. In our experiment we have chosen F such that an electron with T = 54.5eV travels a distance x = 24.48cm to cross the focal plane where the center of the anode is located. Since, for a given F, eq. 2.6 yields T/x = constant we may write

$$T = 54.5\,eV \frac{x}{24.48\,cm} \tag{2.7}$$

Eq. 2.7 gives the relationship between an electron's laboratory velocity component in the plane of deflection and the x-coordinate of its point of detection on the detector which is located in the focal plane. The electric field between the analyzer plates has only a y-component and the electron's velocity components perpendicular to the y-direction are constant. The z-component of the electron's point of detection is therefore given by

$$z = x\frac{v_z}{v_x} = x\frac{v_z}{v_c \cos 30^{\circ}} \tag{2.8}$$

We now need to derive an expression giving the relationship between an electron's energy in the projectile frame and its point of detection. In order to facilitate this we define a new primed coordinate system, rotated clockwise about the z-axis by 30^{o} as shown in figure 2.6. Note that the x'-direction is the direction of the incident beam. For electrons emitted in the x'-z' plane with $\Delta\theta \approx 0^{o}$ we may write the kinetic energy in the projectile frame as

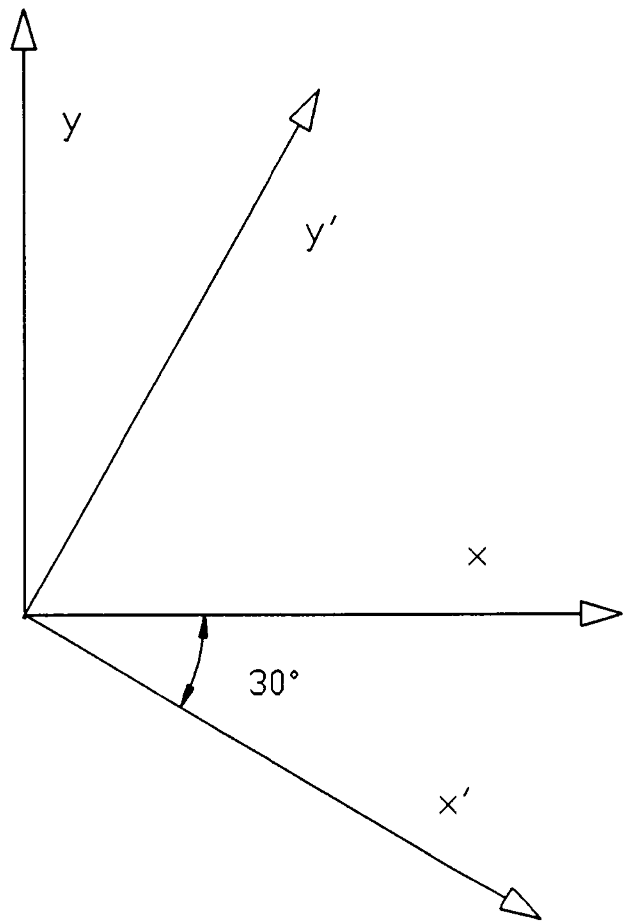

Figure 2.6 Relationship between the original and the primed coordinate system

$$T_{proj}=\frac{1}{2}m_e(v_z'^2+v_{x'proj}^2) \qquad (2.9)$$

where

$$v_{x'proj}=v_{x'lab}-v_{ion} \qquad (2.10)$$

and $v_{z'} = v_z$ is the electron's velocity component perpendicular to the plane of deflection in both the laboratory and the projectile frame. We first express $v_{x'proj.}$ of eq.2.10 in terms of T.

$$v_{x'proj.}=\sqrt{\left(\frac{2T}{m_e}\right)}-\sqrt{\left(\frac{2\cdot 54.5eV}{m_e}\right)} \qquad (2.11)$$

Inserting equations 2.8 and 2.11 into equation 2.9 we obtain, with the help of equations 2.7 and 2.2,

$$T_{proj}=54.5[\frac{z^2\cos^2(30^o)}{Dx}+\frac{x}{D}-\sqrt{\left(\frac{4x}{D}\right)}+1] \qquad (2.12)$$

where D = 24.48 cm. Eq. 2.12 gives the electron's kinetic energy in the projectile frame in terms of the coordinates of its point of deflection for $\Delta\Theta = 0$. Without this approximation we obtain

$$T_{proj}=54.5eV[\frac{z^2\cos^2(30^o+\Delta\theta)}{Dx}+\frac{x}{D}-2\cos\Delta\theta\sqrt{\frac{x}{D}}+1] \qquad (2.13)$$

In the diagram of the analyzer, shown in figure 2.7, typical

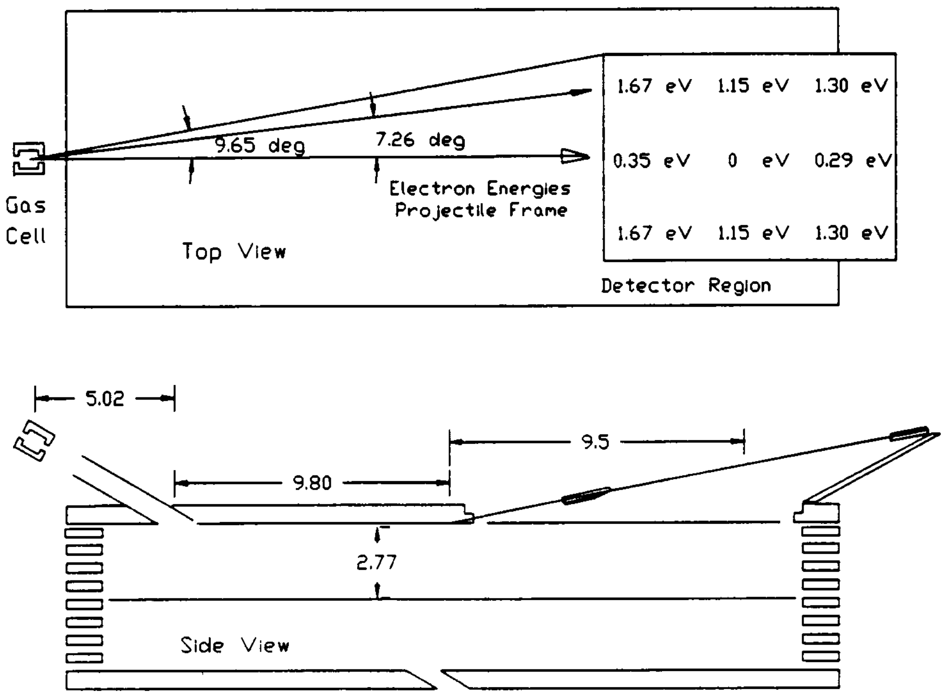

All dimensions are given in centimeters

Figure 2.7 Typical projectile-frame kinetic energies of electrons being detected on different regions of the anode.

projectile frame electron energies are shown, for electrons landing on different regions of the anode.

F. ANODE DESIGN

When an electron emitted with $\Delta\Theta = 0$ arrives at the detector, the x and z coordinates of its arrival position uniquely identify its kinetic energy T_{proj}, as given by eq. 2.12, and its emission angle ϕ defined as

$$\tan\phi = \frac{z \cdot \cos 30^{\circ}}{x - \sqrt{24.48x}} \tag{2.14}$$

The focal plane can therefore be partitioned into several regions, each corresponding to a range of electron energies between $T_{proj}(i)$ and $T_{proj}(i) + \Delta T_{proj}$. Figure 2.8 shows a computer-generated plot of the focal plane partitioned in such a way. We have used this plot as an aid to design electrically-isolated anode segments which will count electrons whose energies and ejection angles in the projectile frame fall into particular ranges. Our anode segments are also shown in figure 2.8. Table 2.2 gives, for each anode segment the range of kinetic energies, the emission angles of electrons detected on this segment and the estimated volume in velocity space intercepted by each segment.

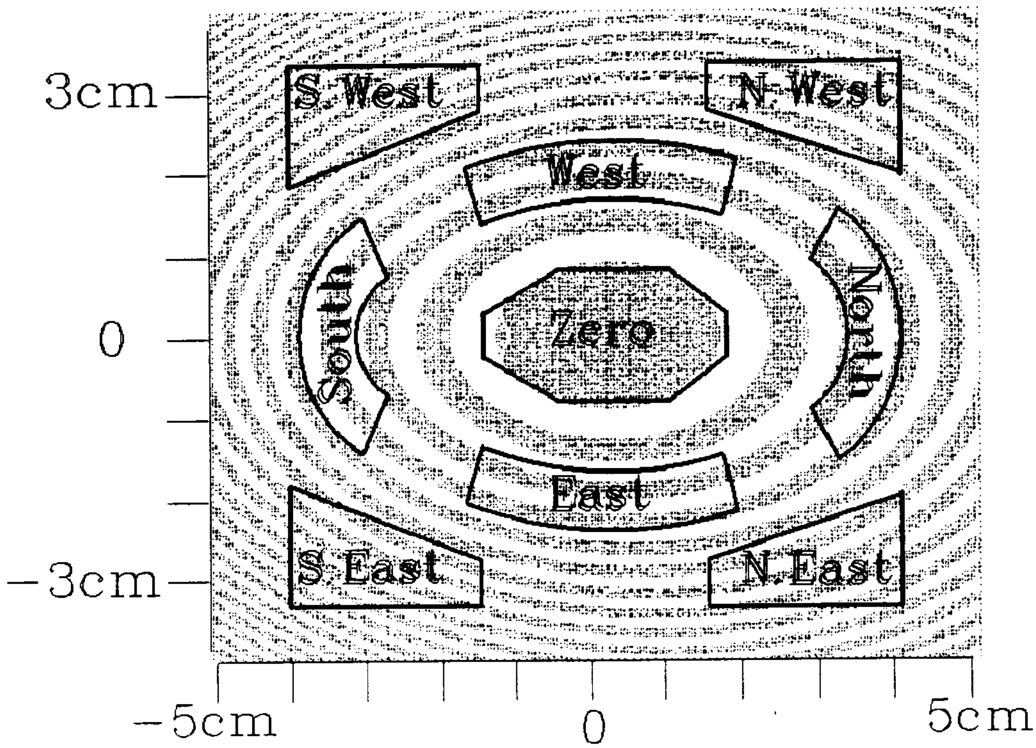

Figure 2.8 The focal plane is partitioned into regions corresponding to arrival positions of electrons with different kinetic energies in the projectile-frame. Successive regions of electron projectile-frame kinetic energies are depicted in increments of 0.05 eV. The anode segments are also shown

Table 2.2

Energy ranges for individual strips

Strip	Energy Range (eV)	Phi Angle Range
Zero	0.0 - 0.05	0° - 360°
E-W	0.18 - 0.35	50° - 141°
South	0.25 - 0.40	148° - 212°
NE-NW	0.47 - 0.76	46° - 73°
SE-SW	0.58 - 0.94	$107_\circ$ - $137_\circ$

Estimated volume in velocity space intercepted by the individual strips

Zero	2.50 ± 0.57	
E-W	2.15 ± 0.49	
South	1.22 ± 0.34	(Units are $10^{-3}au^3$)
NE-NW	1.11 ± 0.28	
SE-SW	1.46 ± 0.31	

G. INDIVIDUAL ANODE STRIP EFFICIENCIES

The entrance aperture of the analyzer, located on the ground-plane allows, electrons emitted with a broad range of emission angles about 30° to enter the analyzer. The exit aperture of the gas cell, however, restricts some of the electrons produced in collisions towards the back of the gas cell from reaching the outer regions of the anode. Only the entrance aperture located in the earth plate of the analyzer is taken into account when the energy and angular ranges given in Table 2.2 are calculated. To account for the restrictions due to the gas cell exit aperture, a program is written to simulate a source of electrons uniformly emitted with a broad range of energies and emission angles all along the intersection between the projectile ion beam and the gas cell. The electrons hitting each strip are counted with and without the gas cell exit aperture in place. We define the efficiency for each strip as the ratio of the number of electrons hitting with the gas cell aperture in place to the number hitting without the gas cell aperture installed. In Table 2.3 we list the efficiencies for the strips used in our experiment.

Table 2.3

Strip efficiencies

Zero	
100 %	
East-West	South-North
100 %	100 %
N.East-N.West	S.East-S.West
97 %	88 %

CHAPTER 3

ELECTRONICS

A. SIGNAL PROCESSING

In this experiment free electrons produced by Ag^{4+} projectile ions colliding with Ar target atoms are detected in coincidence with projectile ions of a selected post-collision charge state. Electrons with energies near 54.5 eV strike the front surface of the microchannel plate electron multiplier. This surface is held at a positive bias voltage of 60 V. The potential difference across the microchannel plate is 1880 V. The anode segments located behind the channelplate are held at 2200 V in a thick copper mounting plate held at 2300 V. When an electron strikes the microchannel plate above an anode segment, the output pulse from the electron multiplier is collected on this segment at high voltage. In order to be processed by front end NIM electronics, the output pulse must be capacitively coupled out of the experimental chamber. The signal lead is connected to one side of the anode segment. To prevent reflections of the output pulse on the opposite side of the anode segment, this side is connected, through a capacitor and a 50 Ω resistor, to ground. Figure 3.1 shows the electrical connections made to each anode segment.

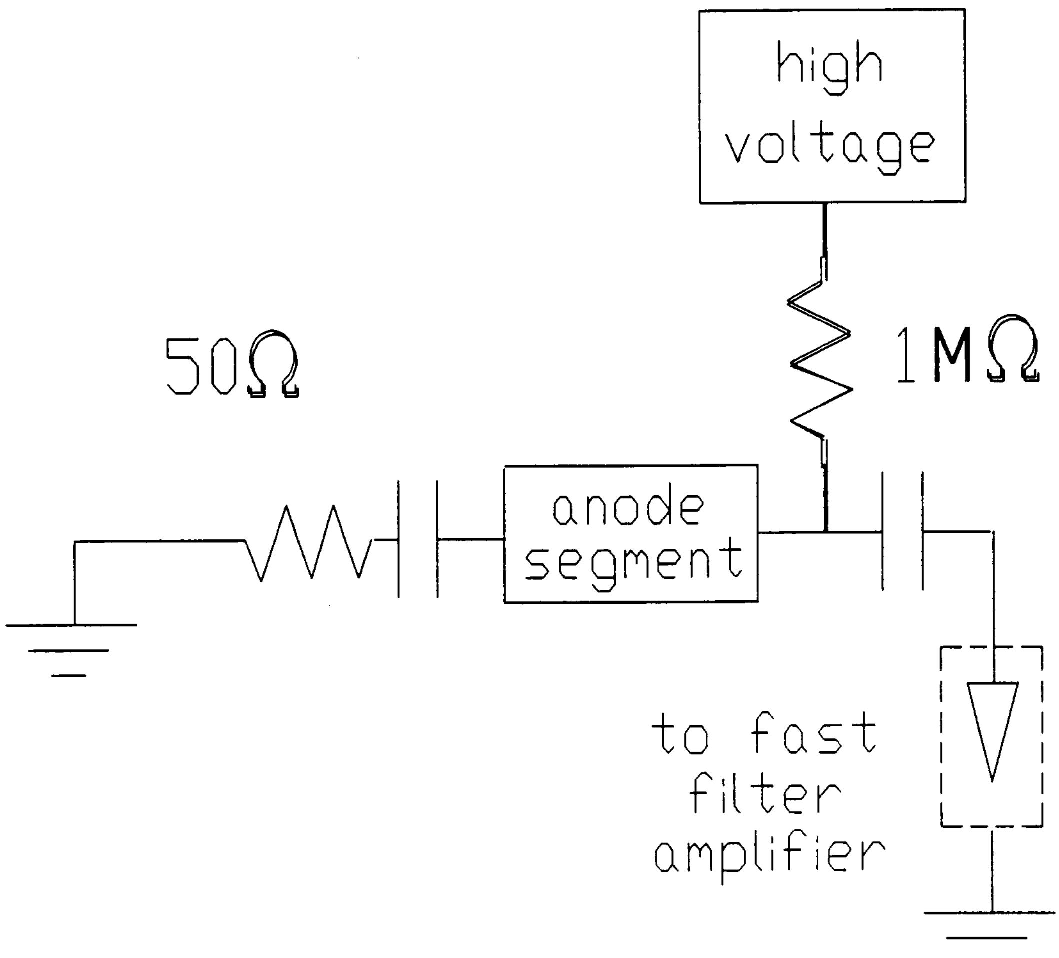

Figure 3.1 Electrical connections made to each anode segment

Projectile ions of the selected charge state strike the first dynode of the discrete dynode electron multiplier. This dynode is biased at ~-3 kV, while the last dynode is grounded. The output pulse of the electron multiplier can therefore be passed directly to the NIM electronics. Output pulses from the multichannel plate and discrete-dynode electron multipliers are current pulses and, when passed through a 50 Ω resistor, result in a voltage pulse of a few millivolts in height and a few nanoseconds in width. All output pulses contain background noise. The pulses are amplified by an ORTEC 863 timing-filter amplifier and then input into a EG&G CG8000 constant-fraction discriminator. The appropriate discriminator level for eliminating noise contributions is determined by observing the amplified output pulses on an oscilloscope. If the minimum voltage amplitude of an amplified pulse exceeds the discriminator level, the discriminator produces a fast NIM output pulse. For counting purposes, the negative NIM output of the discriminators is converted to a positive TTL output by a LRS 688AL level adapter.

B. ELECTRON-ION COINCIDENCES

Free electrons and the projectile ion which produced these electrons reach their respective detectors at different times. To measure electron-ion coincidences, we first determine the difference in the time of detection of an electron and its associated projectile ion. The negative NIM output pulse of a discriminator in the electron counting chain is the START pulse of a time-to-amplitude converter (TAC). The pulse from the discriminator in the ion counting chain is the STOP pulse. If a STOP pulse arrives within a preset time window after a START pulse, the TAC produces an output pulse with an amplitude proportional to the time difference between the START and the STOP pulse. The output pulse of the TAC is fed into an analog-to-digital converter (ADC). Here the amplitude of the input pulse is digitized and its value corresponds to the address of one of the 255 channels of the ADC. Then the counts in this channel are incremented by one. Since the channel number is proportional to the amplitude of the TAC pulse and the amplitude of the TAC pulse, in turn, is proportional to the difference in arrival time between the electron and a projectile ion we can calibrate the ADC spectrum in terms of this difference in arrival time. Figure 3.2 shows the ADC spectrum obtained with electrons detected on the Zero strip as START pulses and Ag^{5+} ion pulses as STOP pulses. A prominent peak appears at ~425 nanoseconds. This peak flags real, as opposed to random coincidences, i.e. the electron and the ion resulted from the same collision. In contrast, random coincidences produce a near uniform background. The difference in the time of detection of an electron and its

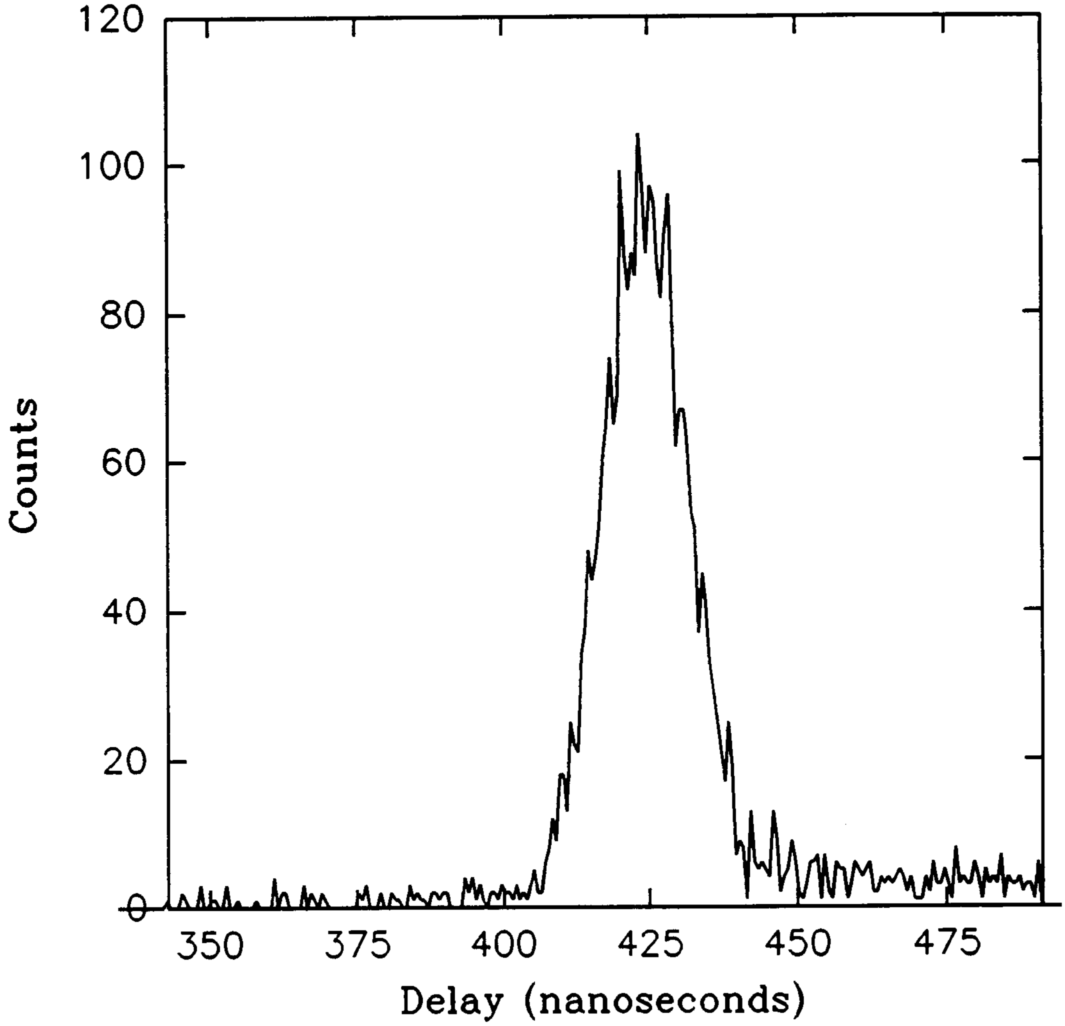

Figure 3.2 An ADC spectrum showing the time difference between electron pulses (as START pulses) and ion pulses (as STOP pulses) to the TAC. The electron is detected ~425 ns before the projectile ion

associated ion is therefore ~425 nanoseconds. The output pulses of the electron discriminator are therefore delayed by 425 ns and stretched, to ensure that they overlap the output pulse of the ion discriminator produced by an associated projectile ion. Both pulses are fed into an EG&G CO 4010 Logic Unit configured as an AND gate which generates a fast negative NIM output pulse whenever two pulses overlap, i.e. whenever an electron-ion coincidence has been detected. After conversion to TTL these pulses are counted, in scalars. Figure 3.3 shows a diagram of the electron-ion coincidence electronics. Enough electronics was available to count electron-ion coincidences for seven anode segments simultaneously.

C. ELECTRON-ELECTRON-ION COINCIDENCES

Our triple coincidence measurements consist of measuring coincidences between electron-ion coincidences measured on the center segment of the anode, (e_o-q), and electron-ion coincidences measured on any one of the six other segments of the anode, (e-q). We refer to these triple coincidence measurements as (e_o-e-q) measurements. To make (e_o-e-q) measurements the (e_o-q) fast negative NIM pulse, from the logic unit, is used as the START pulse for a TAC. The STOP pulse is the (e-q) fast negative NIM pulse which is delayed ~100 nanoseconds using a EG&G GG8000 Octal

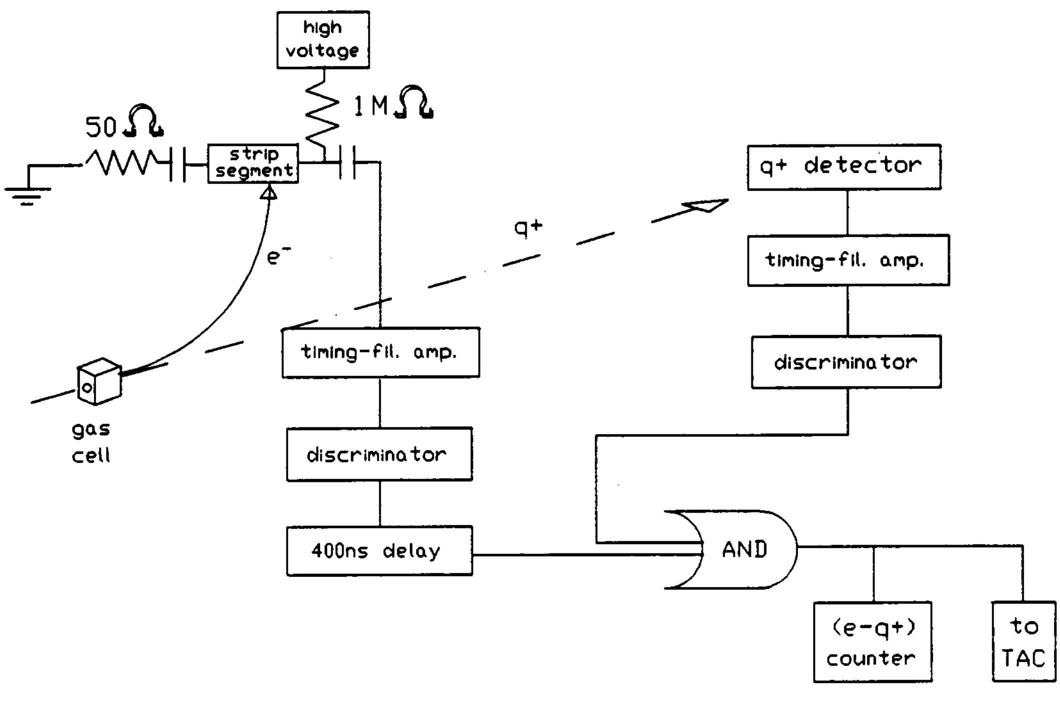

Figure 3.3 A diagram of the electron-ion coincidence electronics

Gate and Delay Generator. The delay ensures that even if the (e-q) pulse from its logic unit comes a few nanoseconds before the accompanying (e_o-q) pulse, the TAC STOP pulse will arrive after the START pulse. This ensures that a coincidence is measured whether the (e_o-q) pulse from the logic unit comes slightly before the (e-q) pulse from the logic unit, or vice versa. Figure 3.4 shows a diagram of the electronics used to make triple coincidence measurements. Figure 3.5 shows a ADC spectrum of (e_o-e-5) TAC pulses with (e_o-5) coincidences from the Zero strip as START pulses and (e-5) coincidences from the East strip as STOP pulses. The broad peak flags the real coincidences, i.e. coincidences between e_o and e electrons, both originating from the same collision which also produced an Ag^{5+} projectile ion. The uniform background to the left of the peak is due to random coincidences. The narrow peak at 57 nanoseconds is the result of electrical noise or cross talk. Triple coincidence measurements were made with (e-q) pulses from the East, West, South, S.West, N.East and N.West strips.

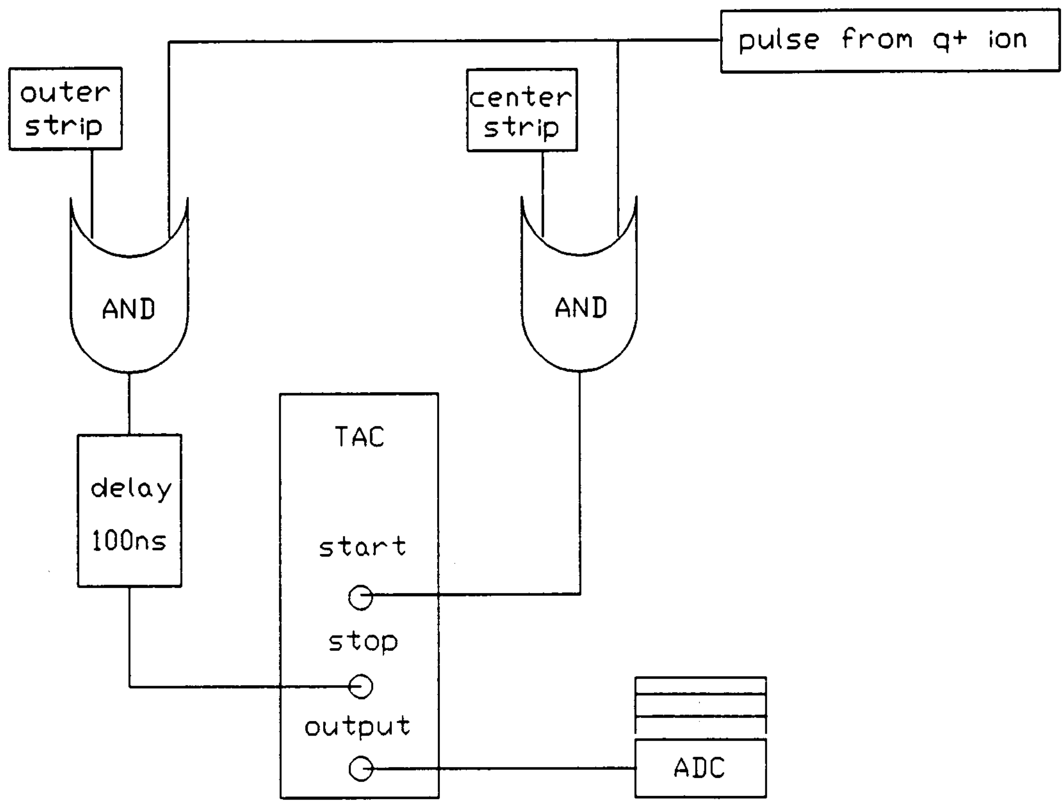

Figure 3.4 A diagrm indicating the electronics used to detect (e_o-e-q) coincidences.

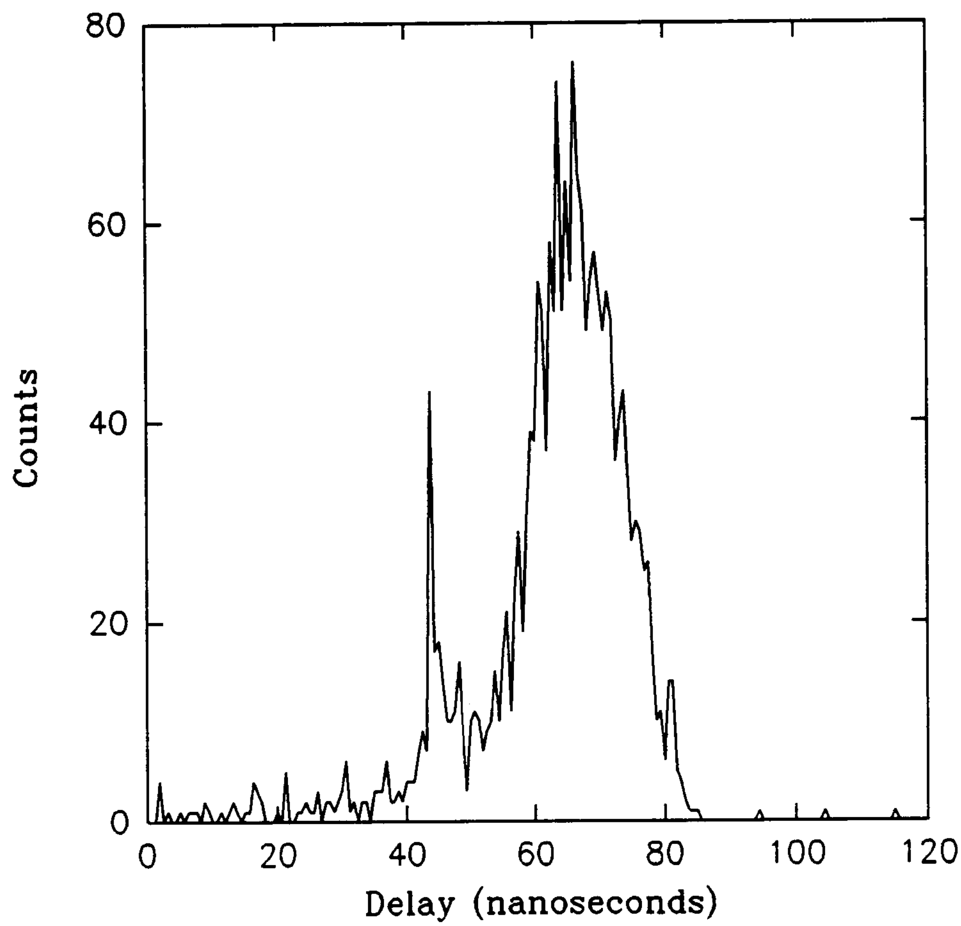

Figure 3.5 TAC spectrum of (e_o-5) events in coincidence with (e-5) events on the East strip.

CHAPTER 4

DATA ANALYSIS

A. OVERVIEW OF THE MEASUREMENTS

In this experiment free electrons produced by Ag^{4+} projectile ions colliding with Ar target atoms are detected in coincidence with projectile ions of a selected post-collision charge state. In the beginning of the experiment we measure the energy spectrum of cusp electrons landing on the Zero strip without any coincidence requirement. This spectrum is shown in figure 4.1. We use this spectrum to determine the voltage on the 30° analyzer, for which electrons, moving with the same velocity as the projectile ion, having 54.5 eV kinetic energy, will land in the center of the Zero strip. For the remainder of the experiment we set this analyzer voltage at 16.38 volts. Then with the analyzer voltage fixed for four target gas pressures, 0.143, 0.561, 0.204, and 0.220 millitorr, we measure, the number of (e-q) coincidences for seven strips and the number of (e_o-e-q) coincidences for the six possible combinations involving the Zero strip and one of the other strips. We normalize these measurements to the number of Ag ions of exit charge state q. Two post-collision charge states, q=5 and q=6, are used for these coincidence measurements. We finish our

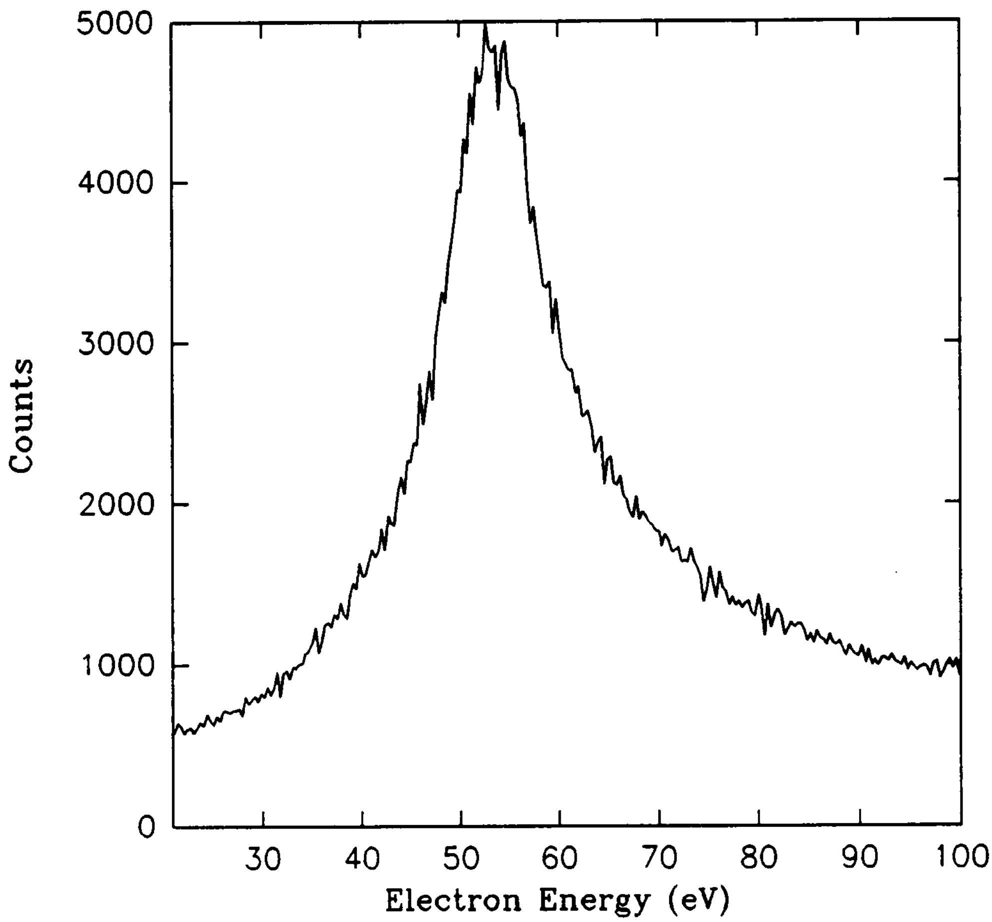

Figure 4.1 Energy spectrum of cusp electrons measured on the Zero strip

experiment by measuring the total number of electrons landing on the Zero strip normalized to the total number of projectiles of post-collision charge state q with q = 3, 4, 5, 6 and 7, and also normalized to the total charge collected in a Faraday cup, at the same four gas pressures and at the background pressure when no Ar gas is admitted to the gas cell. The latter measurements are necessary to determine the exit charge state fractions as a function of the target gas pressure.

B. EXIT CHARGE STATE FRACTIONS

All measurements are normalized to the number of ions of one particular exit charge state q. To obtain absolute cross sections from these measurements the data need to be normalized to the total number of ions that exit the collision region. If the ratio of the number of ions of one exit charge state q to the total number of exiting ions is determined for each of the target gas pressures used, then such a renormalization is possible. Procedures to determine this ratio are explained in the next paragraph.

The ratio of the number of ions of one exit charge state q to the total number of exiting ions is referred to as the charge state fraction, f(q). In our experiment the charge state fractions, f(q,p), are functions of gas pressure. During the experiment the pressure p in the gas feed line leading to the target gas cell is monitored. This pressure is proportional, but not equal to, the absolute pressure in the target gas cell. Because charge exchange cross sections for Ag^{4+} on Ar are known from a previous experiment, the absolute pressure in the gas cell can be determined once the exit charge state fractions for each relative pressure have been found.[28] The total number of cusp electrons produced is directly proportional to the total number of projectile ions passing through the collision region for any fixed relative pressure. At each fixed pressure p we measure the total number of cusp electrons produced, normalized to the number of ions of one exit charge state q by counting the number of ions of exit charge state q in a single ion detector and calculate

$$f'(q) = \frac{\#\ of\ ions\ of\ charge\ q}{\#\ of\ cusp\ electrons} \tag{4.1}$$

We repeat the measurement and normalize to the total number of exiting ions which is determined from the total charge collected in the Faraday cup when the voltage on the charge state analyzer is turned off. From this we calculate.

$$f''(q) = \frac{total\ \#\ of\ ions}{\#\ of\ cusp\ electrons} \tag{4.2}$$

Provided the ion detection efficiencies are equal, the charge state fraction f(q) is obtained by dividing f' by f''. While the detection efficiency of the Faraday cup is assumed to be one, the detection efficiency of the single ion counter is found to be less than unity. Once this detection efficiency is known, absolute charge state fractions can be obtained from the measurements described above. The measurements, however, independently yield relative charge state fractions as a function of relative pressure for each charge state q.

We also compute the charge state fractions f(q) from measurements of f'(q) alone for each exiting charge state q. f'(q) is proportional to the charge state fraction f(q). For each target gas pressure, the sum over q of all charge state fractions, f(q) must equal unity, i.e.

$$\sum_q f(q) = 1 \tag{4.3}$$

since

$$f(q) = (Const.) \cdot f'(q) \tag{4.4}$$

we have

$$\frac{f'(q)}{\sum_q f'(q)} = \frac{\left(\frac{1}{Const.}\right) \cdot f(q)}{\left(\frac{1}{Const.}\right) \cdot \sum_q f(q)} = f(q) \tag{4.5}$$

Under single collision conditions, the probability that an incident projectile ion changes its charge from 4 to q is given by:

$$P(4-q,p) = \sigma(4-q) \cdot n \cdot \ell \cdot p \tag{4.6}$$

where n is the number of target atoms per cm^3 per unit relative pressure, $\sigma(4-q)$ is the charge exchange cross section, ℓ is the effective target gas cell length and p is the relative gas pressure. Therefore under single collision conditions, each charge state fraction f(q,p) varies linearly with gas pressure and for $q \neq 4$ is given by

$$f(q,p) = P(4-q,p) + B(q) = A(q) \cdot p + B(q) \tag{4.7}$$

where B(q) is the charge state fraction at the background pressure.

Measurements needed to compute charge state fractions are made at five different relative target gas pressures, including zero pressure where no argon is let into the gas cell. The charge state fractions are then plotted versus the relative pressure and are fit to a straight line. A(q) is then the slope of the straight line fit and B(q) is the zero-pressure intercept. Two typical fits are shown in figure 4.2. Because the data are fit well by straight lines, we are assured that for this range of relative gas pressures single collision conditions prevail.

The probability, P(4-q) may also be expressed in terms of the absolute pressure p_a.

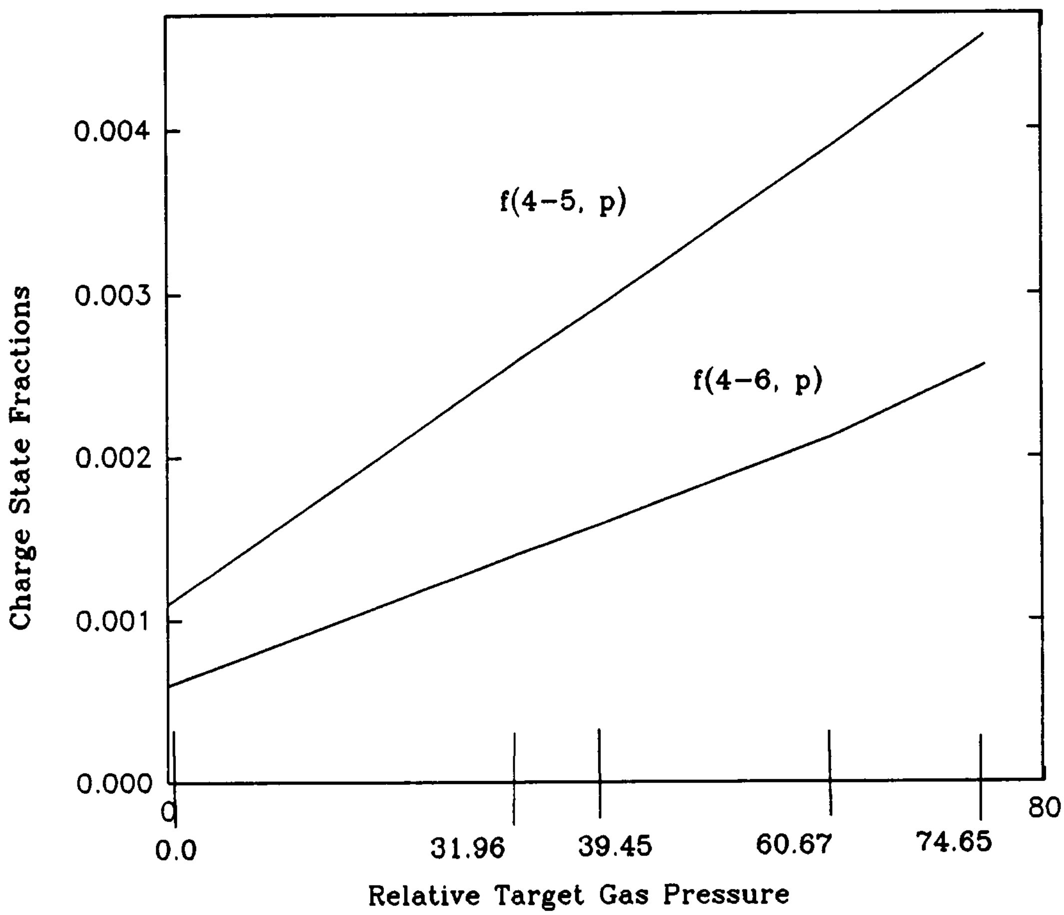

Figure 4.2 Plot of measured charge state fractions versus relative target gas pressure.

$$P(4-q,p_a)=\sigma(4-q)\cdot n_o\cdot \ell\cdot p_a = A_a(q)\cdot p_a \qquad (4.8)$$

where

$$A_a(q)=\sigma(4-q)\cdot n_o\cdot \ell \qquad (4.9)$$

Now n_o is the number of target atoms per cm^3 per millitorr and p_a is the absolute pressure in millitorr. If $\sigma(4-q)$ is known then $A_a(q)$ can be calculated from eq. 4.9 and we obtain

$$p_a=\frac{A(q)\cdot p}{A_a(q)} \qquad (4.10)$$

The cross sections $\sigma(4-3)$, $\sigma(4-5)$, and $\sigma(4-6)$ from reference 28 are now used to compute the absolute pressure p_a corresponding to the relative pressure p. The conversion is found to be

$$\text{Abs.Gas Pres.}=(3.62\pm0.59)\cdot 10^{-3}\cdot \text{Rel.Gas Pres.} \qquad (4.11)$$

C. (e-q) CROSS SECTIONS

The probability that a projectile ion produces an (e-q) event under single collision conditions is expressed as

$$P(e\text{-}q,p_a)=\sigma(e\text{-}q)\cdot n_o\cdot p_a\cdot \ell \qquad (4.12)$$

where n_o, p_a, and ℓ are the same as in eq. 4.8 and σ(e-q) is the partial cross section for (e-q) events. We measure the number of electrons landing on a particular strip in coincidence with an ion of exit charge state q normalized to the total number of ions of exit charge state q. To obtain P(e-q,p_a), we renormalize the measured number of (e-q) events to the total number of ions of all exit charge states for each fixed target gas pressure.

$$P(e\text{-}q,p_a)=\frac{(\#\ of\ (e\text{-}q,p_a))}{(\#\ of\ ions\ of\ charge\ q)}\cdot f(q,p_a) \qquad (4.13)$$

f(q,p_a) is the charge state fraction at the absolute target gas pressure p_a. From eq. 4.12 it follows that, under single collision conditions, P(e-q,p_a) plotted versus the absolute target gas pressure, p_a, may be fitted to a straight line of the form

$$P(e\text{-}q,p_a)=A_a(e\text{-}q)\cdot p_a. \qquad (4.14)$$

with

$$A_a(e\text{-}q)=\sigma(e\text{-}q)\cdot n_o\cdot \ell \qquad (4.15)$$

The slope A_a(e-q) obtained from such a fit then yields the production cross section

$$\sigma(e\text{-}q) = \frac{A_a(e\text{-}q)}{n_o \cdot \ell} \qquad (4.16)$$

We measure electrons in coincidence with the exit charge states q=5 and q=6. The plot of probability versus target gas pressure is well fit to a straight line for each strip for which (e-q) coincidences were measured. Figure 4.3 shows such a fit for $P(e\text{-}5,p_a)$ measured on the East strip.

The number of (e-q) coincidences measured on any strip also includes random coincidences. The number of random coincidences is estimated from

$$\frac{\text{Random Events}}{\text{Real Events}} = \frac{N \cdot \Delta t \cdot (e,p_a)}{(e\text{-}q,p_a)} \qquad (4.17)$$

where N is the number of ions of charge state q counted per second, Δt is the time width of the peak in the TAC spectrum of (e-q) coincidences, (e,p_a) is the total number of electrons striking an anode segment and $(e\text{-}q,p_a)$ is the number of coincidences measured on the same anode segment in a chosen time interval. The estimated number of random coincidences is subtracted from the total number of coincidences measured on each strip before $P(e\text{-}q,p_a)$ is calculated. The corrections for random signals are small,

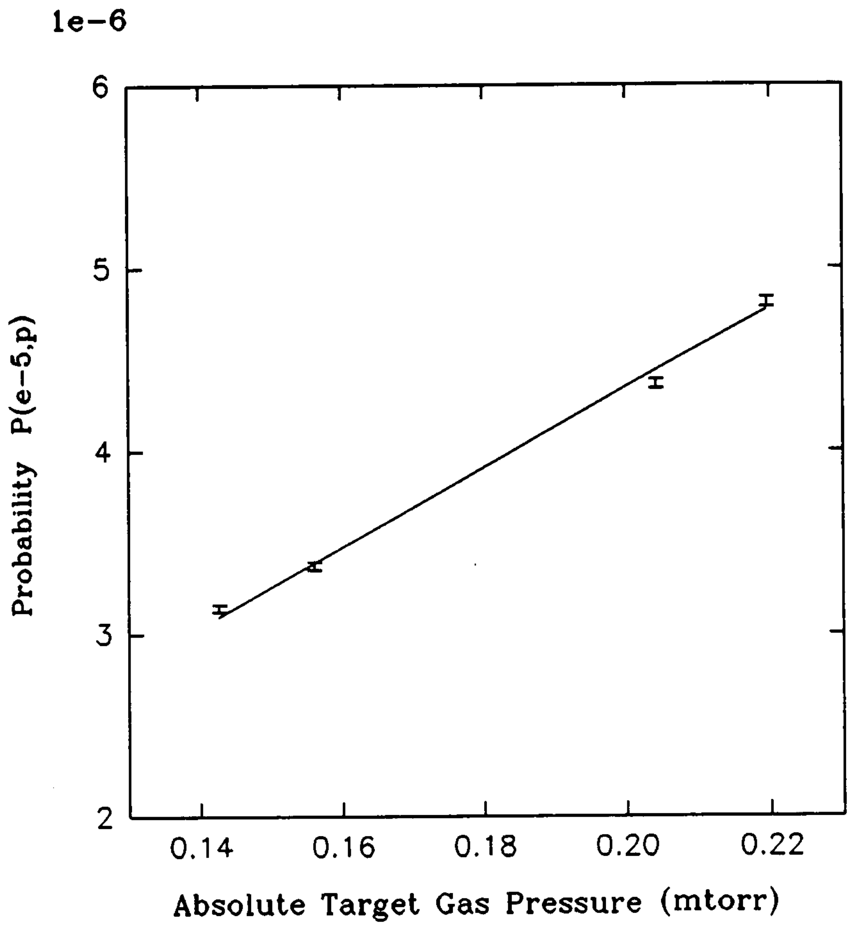

Figure 4.3 A plot of P(e-5,p) versus target gas pressure for cusp electrons measured on the East strip in coincidence with Ag^{5+} ions, and the resulting straight line fit.

being less than 1.5% of the real signal.

D. (e_o-e-q) CROSS SECTIONS

The total number of (e_o-e-q) events is obtained from the number of counts in the peak of an ADC spectrum as shown in figure 3.5. All counts within ± 1/2 full-width-half maximum (FWHM) of the center of the peak are added. The FWHM is determined by fitting the peak in each ADC spectrum to a Gaussian function.

The probability that a projectile ion produces an (e_o-e-q) event under single collision conditions is expressed as

$$P(e_o\text{-}e\text{-}q,p_a)=\sigma(e_o\text{-}e\text{-}q)\cdot n_o\cdot p_a\cdot \ell \tag{4.18}$$

where n_o, p_a and ℓ have been defined previously and σ(e_o-e-q) is the partial cross section for (e_o-e-q) events. Again the measured number of (e_o-e-q) events is normalized to the total number of q ions and we obtain P(e_o-e-q,p_a) from

$$P(e_o\text{-}e\text{-}q,p_a)=\frac{\#\ of\ (e_o\text{-}e\text{-}q,p_a)}{\#\ of\ ions\ of\ charge\ q}\cdot f(q,p_a) \tag{4.19}$$

P(e_o-e-q,p_a), plotted as a function of target gas pressure, may be fit to a straight line of the form

$$P(e_o\text{-}e\text{-}q,p_a)=A(e_o\text{-}e\text{-}q)\cdot p_a \tag{4.20}$$

with

$$A_a(e_o\text{-}e\text{-}q) = \sigma(e_o\text{-}e\text{-}q) \cdot n_o \cdot \ell \tag{4.21}$$

The slope $A_a(e_o\text{-}e\text{-}q)$ obtained from such a fit then yields the production cross section.

$$\sigma(e_o\text{-}e\text{-}q) = \frac{A_a(e_o\text{-}e\text{-}q)}{n_o \cdot \ell} \tag{4.23}$$

Figure 4.4 shows a fit for $P(e_o\text{-}e\text{-}5,p_a)$ for electrons measured between the Zero and East strips.

The $(e_o\text{-}e\text{-}5)$ data fit well to a straight line for those strip combinations for which adequate statistics where available. These are the East-Zero, South-Zero and West-Zero combinations. The S.West-Zero combination has much lower statistics and the fit is not as good. For the N.East-Zero combination we only have data for two different target gas pressures due to an electronic malfunction during the experiment. We therefore must report a large uncertainty in the cross section $\sigma(e_o\text{-}e\text{-}5)$ for the N.East-Zero combination. A large amount of electronic cross talk occurred between the N.West and the Zero strip and we therefore did not calculate the corresponding cross section.

During the experiment we made an additional independent set of measurements of the number of $(e_o\text{-}e\text{-}5)$ coincidences recorded for the various strip combinations as a function of gas pressure. The resulting cross sections, $\sigma(e_o\text{-}e\text{-}5)$, agree with the first set within the quoted uncertainies.

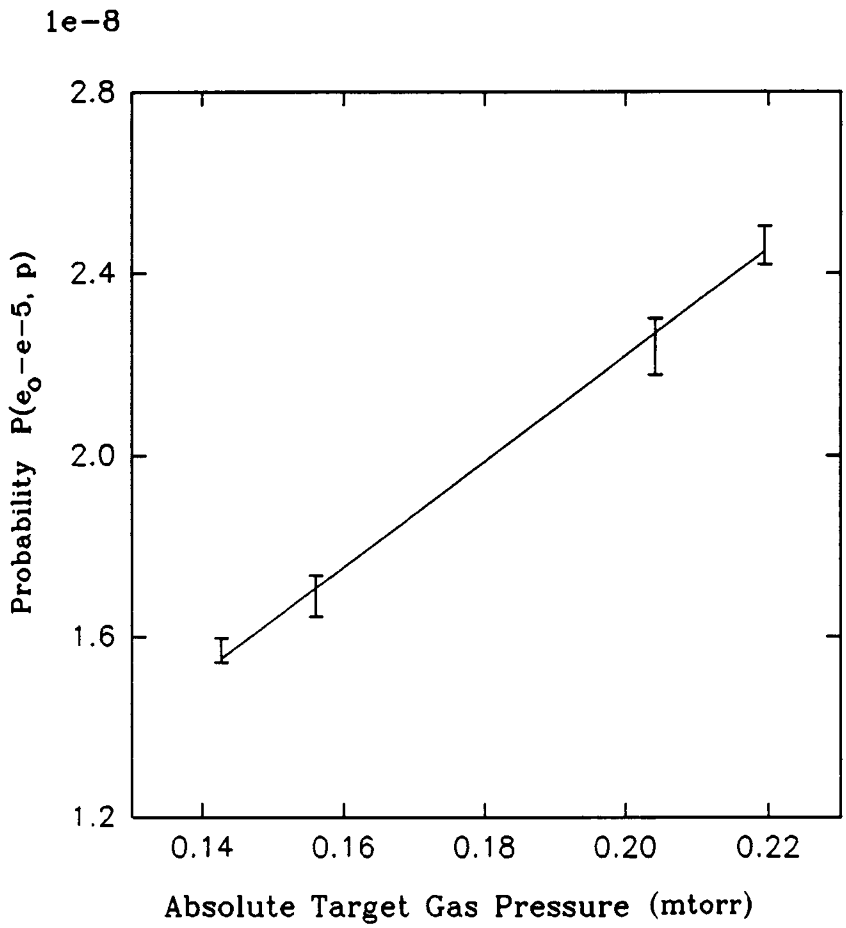

Figure 4.4 A plot of $P(e_o\text{-}e\text{-}5,p_a)$ versus target gas pressure for continuum electrons measured on the East strip in coincidence with continuum electrons measured on the Zero strip in coincidence with Ag^{5+} ions, and the resulting straight line fit.

Similarly, the cross sections obtained for the number of $(e_o$-e-6) coincidences that were measured have the smallest uncertainties for the strip combinations with the highest counting statistics. For the other combinations the uncertainties increase due to lesser counting statistics. Only one set of measurements of the number of $(e_o$-e-6) coincidences as a function of target gas pressure is available.

E. ANALYSIS OF UNCERTAINTIES

In analyzing our data we consider two types of uncertainties: absolute uncertainties, which affect all measurements made during the experiment in the same way, and relative uncertainties, which affect individual measurements only. Absolute uncertainties arise from

(1) The uncertainty in the effective gas cell length, estimated to be ~20%.

(2) The uncertainty in the conversion factor which relates the relative pressure to the absolute pressure, estimated to be ~50%. This estimate takes into account the uncertainties in the measurements of the charge state fractions and the absolute and relative uncertainties in the cross sections used to calculate the conversion factor.

(3) The uncertainty in the transmission efficiency of our 30^{o} electron energy analyzer. The transmission efficiency

is estimated to be to be 96±4%

(4) The uncertainty in the detection efficiency of the MCP detector. In our cross section calculations we have assumed a detection efficiency of 70±20%.[31]

The overall absolute uncertainties in all our cross sections are therefore estimated to be on the order of ±60%.

Relative uncertainties do not affect all of the cross sections in the same way. Relative uncertainties arise from:

(1) Statistical uncertainties in the number of events counted.

(2) Fluctuations in the target gas pressure.

(3) Uncertainties in the charge state fraction used to renormalize the raw data.

(4) Uncertainties in the detection efficiencies of the individual anode segments, since amplifier gain and discriminator settings were adjusted independently for each anode segment.

These relative uncertainties effect the goodness of the straight line fit of $P(e\text{-}q,p_a)$ and $P(e_o\text{-}e\text{-}q,p_a)$ versus pressure. Since the slope of a fit is proportional to the respective cross section, the relative uncertainty in the slope of the straight line fit computed by the fitting routine represents the relative uncertainty in the cross section. All uncertainties in this paper are propagated quadratically.

CHAPTER 5

RESULTS AND CONCLUSIONS

In this chapter we present the cross sections for the production of projectile ions with core charge states, q = 5 and 6, and two electrons in low lying continuum states in collisions of 0.1 MeV/u Ag^{4+} projectiles with Ar atoms. In the projectile frame one of the electrons moves with an energy < 0.13 eV and therefore lands on the Zero strip of the anode after passing through the 30° analyzer. The other electron, moving in the projectile frame with energy in a range ΔE and emission angle in a range $\Delta\phi$ (as given in table 2.2), lands on one of the strips as listed in table 2.2. The angle ϕ is defined in eq. 2.14. The cross sections for the production of projectile ions with only one electron in a low lying continuum state are also given in this chapter. The projectile frame energy and angular distributions of single electrons in low lying continuum states of the projectile ion are compared to the energy and angular distributions of electrons being detected in coincidence with another electron landing on the Zero strip. The distributions differ, possibly signaling the existence of observable electron correlation effects in this collision system.

A. (e-q) CROSS SECTIONS

The cross sections, $\sigma(e\text{-}q)$, for the production of a single electron in a low lying continuum state of a projectile ion with core charge state q (which lands on one of the seven strips), are given in table 5.1 for core charge states q = 5 and 6. The uncertainties given in this and all following tables are relative uncertainties. The ratio of $\sigma(e_o\text{-}6)$ to $\sigma(e_o\text{-}5)$ obtained from coincidence measurements using the Zero strip is

$$\frac{\sigma(e_o-6)}{\sigma(e_o-5)}=0.69 \pm 0.10 \qquad (5.1)$$

We can compare this ratio to the ratio of the cross sections for the production of cusp electrons measured in coincidence with projectile ions of core charge state q = 5 and q = 6 measured by Underwood et al[28] in a previous experiment using a different experimental apparatus. The results of Underwood et al are

$$\frac{\sigma(cusp+6)}{\sigma(cusp+5)}=0.51 \pm 0.08 \qquad (5.2)$$

where the notation is the same as in the reference 28. The ratios agree within their respective uncertainties. Absolute cross sections given in reference 28 cannot be compared directly to those given in table 5.1 since they

TABLE 5.1

Cross sections, $\sigma(e-q)$, in

units of $10^{-19} cm^2$

Data Set	q	Zero	East	West	South	NE	NW	SW
1st	5	21.0 ± 2.3	6.0 ± 0.3	4.5 ± 0.6	3.6 ± 0.3	1.8 ± 1.1	1.8 ± 0.2	1.3 ± 0.2
2nd	5	22.5 ± 0.5	5.9 ± 0.3	4.5 ± 0.2	3.6 ± 0.2	1.9 ± 0.2	1.9 ± 0.2	1.3 ± 0.1
1st	6	14.6 ± 1.41	3.66 ± 0.17	2.84 ± 0.20	2.43 ± 0.18	1.16 ± 0.08	1.21 ± 0.9	0.85 ± 0.6

refer to a different energy and angular range than that subtended by the Zero strip. They therefore differ by a factor of ~2. We expect the cross sections σ(e-q) for the East and West strips and for the N.East and N.West strips to be equal due to the symmetry of the anode design. The observed differences can be due to slight misalignments, stray fields, or variations in detection efficiencies for different strips. For each strip the amplifier gain and the discriminator settings are adjusted independently.

In table 5.1 the cusp shape appears transverse, more electrons land on the East and West than on the South strip, i.e. more electrons seem to be ejected perpendicular to the beam direction than antiparallel to the beam direction in the projectile frame. However the East and West strips intercept larger volumes in velocity space than the South strip. In table 5.2 we present the same cross sections given in table 5.1 normalized per unit volume in velocity space. The cross sections measured on each strip have been divided by the volume in velocity space intercepted by that strip. In table 5.2 the cusp no longer appears transverse.

TABLE 5.2

Cross sections, $\sigma(e-q)$,
per unit volume in velocity space
in units of $10^{-16} cm^2 au^{-3}$

Data Set	q	Zero	East	West	South	NE	NW	SW
1st	5	8.4 ± 2.3	2.9 ± 0.6	2.1 ± 0.5	3.0 ± 0.9	1.5 ± 1.1	1.5 ± 0.5	1.28 ± 0.27
2nd	5	9.0 ± 2.1	2.7 ± 0.6	2.1 ± 0.5	3.0 ± 0.9	1.8 ± 0.5	1.8 ± 0.5	1.28 ± 0.27
1st	6	5.84 ± 1.34	1.70 ± 0.39	1.32 ± 0.30	2.00 ± 0.56	1.05 ± 0.27	1.1 ± 0.28	0.88 ± 0.19

B. (e_o-e-q) CROSS SECTIONS

The cross sections, $\sigma(e_o\text{-e-q})$, for the production of two electrons in low lying continuum states of a projectile ion with core charge state q, when one electron lands on the Zero strip and the other electron lands on one of the other strips, are given in table 5.3. As with (e-q) events, we expect the cross sections $\sigma(e_o\text{-e-q})$ for the East and West strips to be equal due to the symmetry of the anode design. Again, observed differences can be due to slight misalignments, stray fields, or variations in detection efficiencies for different strips.

In table 5.4 we present the same cross sections per unit volume in velocity space and in table 5.5 we present the ratio of the cross sections, $\sigma(e_o\text{-e-q})/\sigma(\text{e-q})$. We note that in contrast to the cusp resulting from (e-5) events, the cusp resulting from (e_o-e-5) events appears transverse. When two electrons are found in low-lying continuum states of the projectile ion after a collision of a Ag^{4+} projectile with an Ar atom and one of the electrons moves very slowly in the projectile frame with a kinetic energy of less than 0.13 eV, then the other electron is more likely to move perpendicular to the beam direction than antiparallel to the beam direction. This tendency is stronger for two electrons in low-lying continuum states of a Ag^{5+} ion than for two electrons in low-lying continuum states of a Ag^{6+} ion. We

TABLE 5.3

Cross sections, $\sigma(e_o\text{-}e\text{-}q)$, in units of 10^{-22} cm^2

Data Set	q	East	West	South	NE	SW
1st	5	32.1 ± 1.7	27.3 ± 1.7	10.7 ± 0.9	5.5 ± 1.9	5.1 ± 0.7
2nd	5	31.1 ± 2.3	27.9 ± 2.1	10.7 ± 1.4	7.3 ± 1.1	7.2 ± 1.3
1st	6	21.8 ± 0.6	18.6 ± 0.6	8.3 ± 0.3	4.5 ± 0.3	4.8 ± 0.3

TABLE 5.4

Cross sections, $\sigma(e_0\text{-}e\text{-}q)$,
per unit volume in velocity space
in units of $10^{-19}cm^2au^{-3}$

Data Set	q	East	West	South	NE	SW
1st	5	15.0 ± 3.5	12.8 ± 3.0	8.7 ± 2.4	4.9 ± 2.2	3.6 ± 0.9
2nd	5	15.0 ± 3.3	13.1 ± 3.0	8.7 ± 2.4	6.5 ± 1.5	5.0 ± 1.0
1st	6	10.1 ± 2.4	8.7 ± 2.0	6.8 ± 2.0	4.0 ± 1.1	3.3 ± 0.7

TABLE 5.5

Ratio of $\sigma(e_o\text{-}e\text{-}q)$ to $\sigma(e\text{-}q)$ for q = 5 and 6 multiplied by 10^3.

Data Set	q	East	West	South	NE	SW
1st	5	5.15 ± 0.47	6.24 ± 0.74	3.12 ± 0.17	3.32 ± 0.11	2.72 ± 0.61
2nd	5	5.37 ± 0.28	6.53 ± 0.92	2.95 ± 0.30	4.05 ± 0.62	3.74 ± 0.59
1st	6	5.94 ± 0.53	6.46 ± 0.75	3.29 ± 0.36	3.80 ± 0.71	3.63 ± 0.35

note that for a Ag^{5+} ion, electrons in low-lying continuum states are produced by a capture-plus-ionization event, while for a Ag^{6+} ion they are produced by a double-ionization event.

C. FIT TO THE CUSP SPECTRUM IN FIGURE 4.1

In this section we take a closer look at the energy spectrum of cusp electrons measured on the Zero strip without any coincidence requirement, shown in figure 4.1. We can use this energy spectrum to experimentally verify the calculated energy resolution and angular acceptance of the 30° analyzer. Our measured spectrum gives us the number of electrons detected as a function of their laboratory frame energy E or their laboratory frame velocity v. We may denote it by Q(v). To relate this measured distribution Q(v) to the doubly differential cross section for cusp electrons, $d\sigma/d\vec{v}'$, where $\vec{v}'$ is the velocity of the cusp electron in the projectile frame, we must consider the spectrometer resolution function $S(v,\Omega)$ and integrate $d\sigma/d\vec{v}'$ over the experimental acceptances in velocity and angle.

$$Q(v_o) = \int_v\int_\Omega S(v,\Omega)\, v^2 \frac{d\sigma}{d\vec{v}'}\, dv\, d\Omega \tag{5.3}$$

For the Zero strip, $S(v,\Omega)$ depends on v and on the emission angle Θ with respect to the beam axis in the laboratory frame but is nearly independent of the azimuthal angle ϕ. We approximate further by assuming that $S(v,\Omega)$ may be written as $S(v,\Omega) = G(\Theta)\cdot H(v)$ where $G(\Theta)$ is constant for $0 \leq \Theta \leq \Theta_o$

$$G(\theta) = \Theta(\theta)\cdot\Theta(\theta_o - \theta) \tag{5.4}$$

and $H(v)$ is constant for $(1-\rho)v_o < v < (1+\rho)v_o$

$$H(v) = \Theta(v-(1-\rho)v_o)\cdot\Theta((1+\rho)v_o - v) \tag{5.5}$$

The differential cross section, $d\sigma/d\vec{v}'$, may be expressed in a projectile frame partial wave expansion.[33] If the coefficients in this expansion are then represented in a power series we obtain

$$\frac{d\sigma}{d\vec{v}'} = \frac{1}{v'}\sum_{n,j=0}^{\infty} v'^{n} P_j(\cos\theta')\, B_{jn}(v_i) \tag{5.6}$$

where v' is the velocity of the electron in the frame of the projectile, $P_j(\cos\Theta')$ are Legendre polynomials of order j, Θ' is the angle the electron makes with the beam axis in the frame of the projectile and $B_{jn}(v_i)$ are the coefficients of the expansion which vary with the velocity of the projectile ion, v_i. Inserting eq. 5.6 in our expression for $Q(v)$ we obtain

$$Q(v_o) = \sum_{n,j=0}^{\infty} B_{jn}(v_i)\, U_{jn}(v_o) \tag{5.7}$$

where

$$U_{jn}(v) = 2\pi \int_{(1-\rho)v}^{(1+\rho)v} \int_0^{\theta_o} v^2 v'^{\,n-1} P_j(\cos\theta')\, dv \sin\theta d\theta \tag{5.8}$$

We try to obtain a good fit to our spectrum with the minimum number of coefficients, B_{jn} plus a constant term, C to represent the background. The acceptance angle θ_o, the parameter ρ defining the velocity resolution, the coefficients B_{jn}, and the constant term C will be adjusted by a fitting program adapted from Bevington[32] to yield the best fit to the cusp in figure 4.1. Let us write

$$Q(v_o) = C + Q_{00}(v_o) + Q_{10}(v_o) + Q_{20}(v_o) + Q_{01}(v_o) + \cdots \tag{5.9}$$

The expression for the monopole term, Q_{00}, is

$$Q_{00}(v_o) = 2\pi \int_{(1-\rho)v}^{(1+\rho)v} \int_0^{\theta_o} \frac{B_{00}}{v'} v^2 dv \sin\theta d\theta \tag{5.10}$$

In order to evaluate the integral we express v' in terms of v and v_i with

$$v' = \sqrt{v^2 + v_i^2 - 2 \cdot v \cdot v_i \cdot \cos\theta} \tag{5.11}$$

then

$$Q_{00}(v_o) = 2\pi B_{00}\left[\frac{1}{3v_i}v'^{\frac{3}{2}} + \right. \tag{5.12}$$

$$\left.\cos\theta\left((v-v_i\cos\theta)\frac{v'^{\frac{1}{2}}}{2}+\frac{v_i^2\sin^2\theta}{2}\ln\left(v-v_i\cos\theta+\sqrt{v'}\right)\right)\right]\Bigg|_0^{\theta_o}\Bigg|_{(1-\rho)v_0}^{(1+\rho)v_o}$$

The Q_{01} term can also be easily integrated.

$$Q_{01}=2\pi\ B_{01}\int_{(1-\rho)v_0}^{(1+\rho)v_0}\int_0^{\theta_0}\sin\theta d\theta v^2 dv \tag{5.13}$$

The integral is straightforward and becomes

$$Q_{01}=\left[-\frac{2}{3}\pi\cdot B_{01}\cdot v^3\cdot\cos\theta\right]\Bigg|_0^{\theta_0}\Bigg|_{(1-\rho)v_0}^{(1+\rho)v_0} \tag{5.14}$$

The dipole term, Q_{10} and the quadrupole term, Q_{20} are given by

$$Q_{10}=2\pi B_{01}\int_{(1-\rho)v_0}^{(1+\rho)v_0}\int_0^{\theta_0}\frac{v\cos\theta-v_i}{v^2+v_i^2-2vv_i\cos\theta}v^2dv\sin\theta d\theta \tag{5.15}$$

and

$$Q_{20}=2\pi\cdot B_{20}\int_{(1-\rho)v_0}^{(1+\rho)v_0}\int_0^{\theta_0}\left(\frac{3(v\cos\theta-v_i)^2}{2v'^3}-\frac{1}{2v'}\right)v^2dv\sin\theta d\theta \tag{5.16}$$

These terms are cumbersome to integrate analytically and therefore are integrated numerically.

We try to obtain a good fit to our spectrum with four different functions. The multipole chosen to add to each previous function is the one which improves the fit the most.

Function (1): $Q_{00} + C.$

Function (2): $Q_{00} + Q_{01} + C$

Function (3): $Q_{00} + Q_{01} + Q_{20} + C$

Function (4): $Q_{00} + Q_{01} + Q_{20} + Q_{10} + C$

The best fits obtained with each function are shown in figure 5.1. In table 5.5, the χ^2, Θ_o and ρ parameters, found for the best fit of each of the four functions, are displayed. The function (1) results in a poor fit. More than the monopole term, commonly refered to as the Dettmann cusp plus a constant background, is needed to properly fit our measured spectrum. With the Q_{01} term added the fit improves dramatically as witnessed by the much smaller χ^2 for function (2). The quadrupole term, Q_{20} added to function (3) improves the fit further. Function (4) gives the lowest χ^2, with the dipole term, Q_{10} added. Note that the angular acceptance and energy resolution do not change appreciably for functions 2 through 4. For function (3) and function (4) the angular acceptance is close to the reported value in table 2.1 and the energy resolution is close to what we expect it to be from the analyzer dimensions. We are therefore confident that our analyzer performs as expected and described in chapter 2.

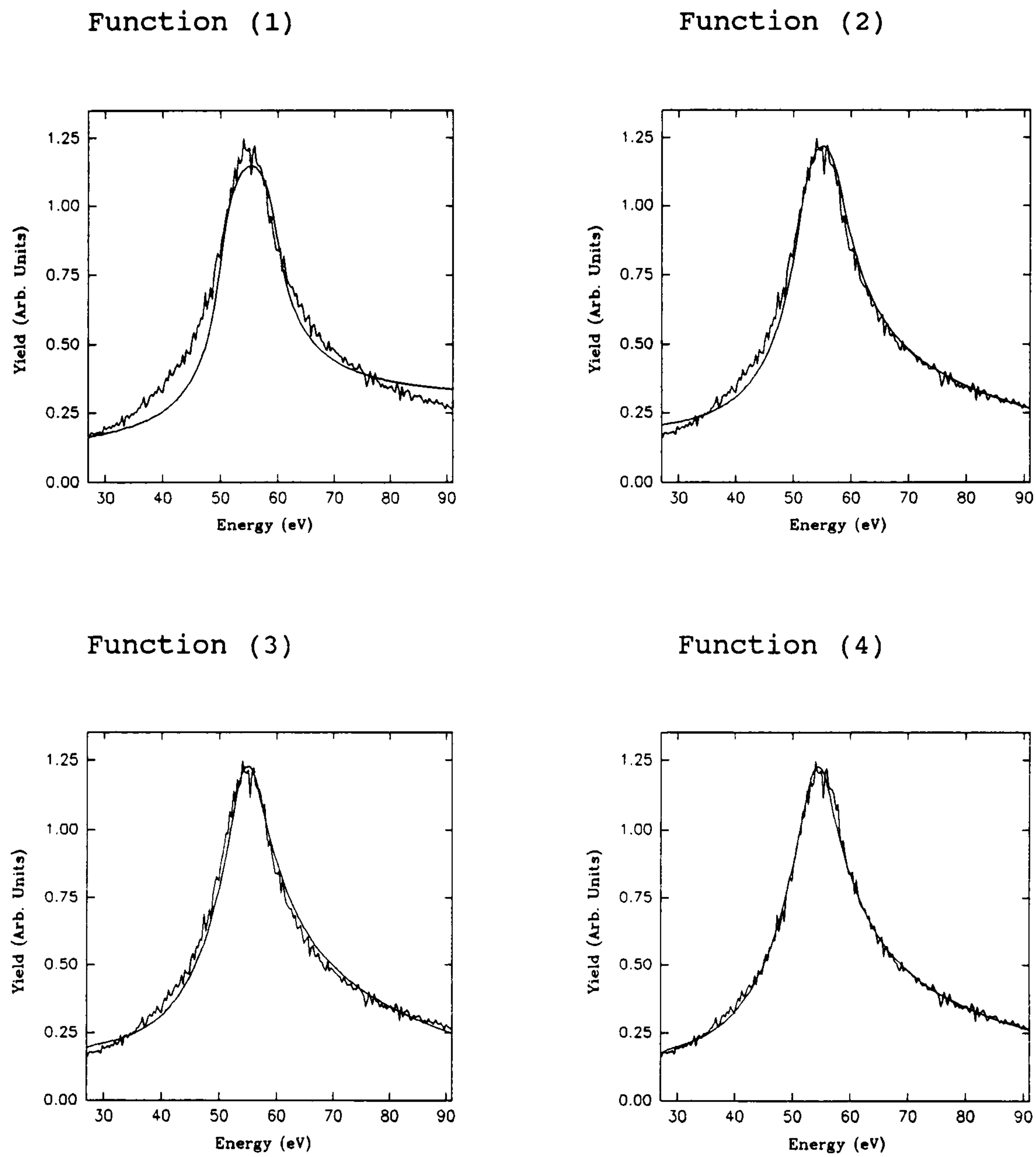

Figure 5.1 Best fits to the measured spectrum obtained with various fitting functions

Table 5.6

Values of fitting parameters.

Function	χ^2	Θ_o	$\rho\times10^{-2}$
1	13.3	1.7^o	4.5
2	3.1	3.3^o	3.3
3	2.9	3.1^o	2.1
4	1.1	3.1^o	2.1

D. CONCLUSIONS

This experiment is a feasibility study. We have shownthat it is possible to detect two electrons in low lying continuum states of a 0.1 MeV/u Ag^{q+} projectile, following a single collision of a 0.1 MeV/u Ag^{4+} projectile with an Ar atom. We have measured the cross sections for producing such states with one electron moving with a kinetic energy less than 0.13 eV in the projectile frame and the other moving with somewhat higher kinetic energy approximately antiparallel or perpendicular to the beam direction. To the best of our knowledge this work is the first to report on having successfully made this kind of measurement. The results of our measurements may signal electron-electron correlation effects. We have shown that electrons moving with kinetic energies between 0.18 eV and 0.35 eV in the projectile frame are more likely to move perpendicular than antiparallel to the beam direction if another very low energy continuum electron is present. Without this coincidence requirement, the angular distribution of electrons in this energy range is more isotropic. Future experiments can now be designed to measure in more detail the energy and angular correlations of two electrons in low-lying continuum states of the projectile. The experimental arrangement can be improved. To aid in setting the gains of the amplifiers for each of the anode segments we will install a resistive anode encoder in place of the anode configuration now in use behind the channel plate. By comparing the number of electrons detected with the resistive anode encoder and the segmented anode we will be able to determine the relative efficiencies of each of the anode segments. The position sensitive detector will also allow us to study the effects of misalignments and stray magnetic fields.

LIST OF REFERENCES

BIBLIOGRAGHY

[1] J.H.McGuire, Phys. Rev. A 36, 1114 (1987)

[2] U.Fano, Rep. Prog. Phys. 46, 97 (1983)

[3] A.R.P.Rau and Q.Molina, J. Phys. B 22, 189 (1989)

[4] E.P. Wigner, Phys. Rev. 73, 9, 1002 (1948)

[5] K.Dettmann, K.G.Harrison and M.W.Luows, J.Phys. B. 7, 269 (1974)

[6] G.H. Wannier, Phys. Rev. 90, 5, 817 (1953)

[7] A.R.P.Rau, The Physics of Electronic and Atomic Collisions, J.Eichler, I.V.Hertel, N.Stolterfoht (eds.) 711 (1984)

[8] A.R.P.Rau, Comments At. Mol. Phys. 14, 6, 285 (1984)

[9] A.R.P.Rau, Nuc. Inst. Meth. B56/57, 200 (1991)

[10] S.Cvejanovic and F.H.Read, J. Phys. B 7, 1841 (1974)

[11] J.B.Donahue, P.A.M.Green, M.V.Hynes and R.W.Hamm, Phys. Rev. Lett. 48, 22, 1538 (1982)

[12] P.Selles, A.Heutz and J.Mazeau, J. Phys. B 20, 5195 (1987)

[13] A.L.Ford and J.F.Reading, Nuc. Inst. Meth. B56/57, 196 (1991)

[14] W.Fritsch, C.D.Lin, Phys. Rev. A 41, 4776 (1990)

[15] L.H.Andersen, P.Hvelplund, H.Knudsen, S.P.Moller, and A.H.Sorensen, Phys. Rev. A 36, 3612 (1987)

[16] J.P.Giese, M.Schulz, J.K.Swenson, H.Schöne, M.Benhenni, S.L.Varghese, C.R.Vane, P.F.Dittner, S.M.Shafroth and S.Datz, Phys. Rev. A 42, 1231 (1990)

[17] A.Skutlartz, S.Hagmann and H.Schmidt-Böcking, J. Phys. B, 21, 3609 (1988)

[18] L.H.Anderson, The Physics of Electronic and Atomic Collisions, D.C.Lorents, W.E.Meyerhof, J.R.Peterson (eds.) 365 (1986)

[19] R.Mann and H.Schulte, Z Phys. D 4, 343 (1987)

[20] N.Stolterfoht, C.C.Havener, R.A.Phaneuf, J.K.Swenson, S.M.Shafroth, and F.W.Meyer, Phys. Rev. Lett. 57, 74 (1986)

[21] F.W.Meyer, D.C.Griffin, C.C.Havener, M.S.Huq, R.A.Phaneuf, J.K.Swenson, and N.Stolterfoht, Electronic and Atomic Collisions, H.B.Gilbody, W.R.Newell, F.H.Read, A.C.H.Smith (eds.) 673 (1988)

[22] J.A.Tanis, G.Schiwietz, D.Schneider, N.Stolterfoht, W.G.Graham, H.Altevogt, R.Kowallik, A.Mattis, B.Skogvall, T.Schneider, and E. Szmola, Phys. Rev. A 39, Rapid Communications, 1571 (1989)

[23] L.H.Andersen, M.Frost, P.Hvelplund, H.Knudsen, and S.Datz, Phys. Rev. Lett. 52, 518 (1984)

[24] S.Datz, R.Hippler, L.H.Andersen, P.F.Dittner, H.Knudsen, H.F.Krause, P.D.Miller, P.L.Pepmiller, T.M.Rosseel, N.Stolterfoht, Y.Yamazaki, and C.R.Vane, Nucl. Instr. Meth. A262, 62 (1987)

[25] H.Damssgaard, H.K.Haugen, P.Hvelplund, and H.Knudsen, Phys. Rev. A 27, 112 (1983)

[26] P.Hvelplund et. al., unpublished

[27] T.A.Underwood, M.Breinig, C.C.Gaither III, and J.Freyou, Phys. Rev. A 38, 6138 (1988)

[28] T.A.Underwood, M.Breinig and C.C.Gaither, Phys. Rev. A 44, 1668 (1991)

[29] T.S.Green and G.A.Proca, Rev. Sci. Inst., 41, 10, 1410 (1970)

[30] J.E.Freyou, Masters Thesis, University of Tennessee, Dec. (1988)

[31] Joseph Ladislas Wisa, Nuc. Inst. Meth. 162, 387 (1979)

[32] P.R.Bevington, Data Reduction and Error Analysis for the Physical Sciences, McGraw-Hill, 1969

[33] W.Mechbach, I.B.Nemirovsky, and C.R.Garibotti, Phys. Rev. A 24, 4 (1981)

VITA

John Dirk Richards was born in Albany, New York on May 16, 1959. He attended Lewisboro elementary school and John Jay High School in the Katonah-Lewisboro school district. In December, 1984, he received a Bachelor's degree in Physics with a minor in Mathematics from the State University of New York at Purchase.

In May 1992, he will officially receive a M.S. in physics from the University of Tennessee. His thesis work concerned experimental atomic collision physics and was conducted within the University of Tennessee Atomic Physics Group at the Oak Ridge National Laboratory EN tandem Van de Graaff accelerator facility.